THE PENNSYLVANIA STATE UNIVERSITY
SCHREYER HONORS COLLEGE

DEPARTMENT OF BIOMEDICAL ENGINEERING

INVESTIGATING THE IMPACT OF FLOW RECIRCULATION ON CELLULAR UPTAKE OF NANOPARTICLES

SAMUEL BOLAND
SPRING 2018

A thesis
submitted in partial fulfillment
of the requirements
for baccalaureate degrees
in Biomedical Engineering & Mechanical Engineering
with honors in Biomedical Engineering

Reviewed and approved* by the following:

Peter Butler, PhD
Associate Dean for Education in The College of Engineering
Professor of Biomedical Engineering
Thesis Supervisor

Justin Brown, PhD
Associate Professor of Biomedical Engineering
Honors Adviser

* Signatures are on file in the Schreyer Honors College.

ABSTRACT

Atherosclerosis is a progressive cardiovascular disease that is the number one killer of people in the developed world. The pathology of atherosclerosis falls at the unique intersection of cellular mechanics, fluid mechanics, and mass transfer. The mechanical properties of cells in highly atherogenic regions of the vasculature are modified by the fluid dynamics, which in turn impacts mass transfer properties from the fluid to the cell. Ironically, the same mechanical and transport conditions that promote growth of atherosclerotic lesions may also provide an avenue for new treatment methods, chiefly the delivery of nanoparticles that might be loaded with drugs to treat atherosclerosis. In this thesis, this phenomenon is computationally and experimentally investigated. A novel flow chamber was manufactured to mirror the conditions of regions highly prone to atherosclerotic plaque. The cellular uptake of nanoparticles was quantified and compared to the uptake of nanoparticles by cells subject to conditions of aligned flow. Computational modeling of this phenomenon was used to drive the design of the flow chamber and support the hypothesis that flow recirculation has a profound impact on cellular uptake of nanoparticles.

TABLE OF CONTENTS

LIST OF FIGURES

LIST OF TABLES

ACKNOWLEDGEMENTS

First and foremost, I would like to thank Dr. Peter Butler, my thesis advisor and principal investigator, for serving as such a positive mentor throughout my four years here. Dr. Butler's support over the past four years has taught me the importance of scientific integrity, the ability to remain level-headed in stressful situations, and problem solving skills that I will take with me for the rest of my life.

Next, I would like to thank Dr. Justin Brown and Dr. James Pawelczyk for serving as members of my thesis committee. Both members of the committee provided valuable advice and guidance throughout the project and their experience was indispensable. Qiong Wei of Dr. Sulin Zhang's lab also served as a valuable resource for porous media. I would also like to thank Dr. Keefe Manning for serving as an excellent mentor to me and for providing a usable peristaltic pump in the eleventh hour to save this project.

I also thank the other members of the Mechanobiology Lab who have contributed to this work, namely Michael King, Nicholas Frazzette, and Seoyoung Son. Mr. King provided the foundation necessary for completing this project. Mr. Frazzette served as a positive role model during my early years in the lab and his honors thesis was consulted often during the writing of this work. Ms. Son was my primary lifeline in the lab, always stepping in when I required guidance. I could not have completed this project without help from these individuals.

Finally, I am thankful for the support of my family throughout my entire undergraduate career. I would like to thank my brothers, Matt and Mark, for being excellent role models throughout my childhood and always pushing me to be my best. I would also like to thank my parents, Carol and Mark, for their unwavering support and belief in me.

Chapter 1

INTRODUCTION TO ATHEROSCLEROSIS

Atherosclerosis is a progressive cardiovascular disease that is characterized by the gradual thickening and stiffening of large arteries within the cardiovascular system. Commonly referred to as heart disease, atherosclerosis becomes more prominent over time as lipids and other fibrous elements are deposited within the vessel wall of large arteries. Accumulation of atherosclerotic lesions is a function of one's diet; high-fat and high-cholesterol diets result in the deposition of lipoproteins within the intima, the middle portion of the vessel wall. These depositions gradually grow inward towards the center of the lumen, occluding blood flow. This thesis demonstrates how the same physics that define the pathology of atherosclerosis may also lead to effective methods of treatment, and how a flow chamber to investigate this phenomenon was manufactured and utilized.

Section 1.1 – Why is Atherosclerosis Worthy of Research?

Atherosclerosis alone does not pose much of a threat. It is when atherosclerosis is combined with thrombosis or plaque rupture that there is truly a risk of a fatal event. As atherosclerosis progresses, the plaque occludes more and more of the lumen, increasing the vessel's susceptibility to a thrombosis. The cross section of a lumen occluded by atherosclerotic plaque, with the lumen stained in blue and plaque stained in red, is provided in figure 1. This occlusion is typical of a late-stage heart disease patient and poses a great risk to cardiovascular health

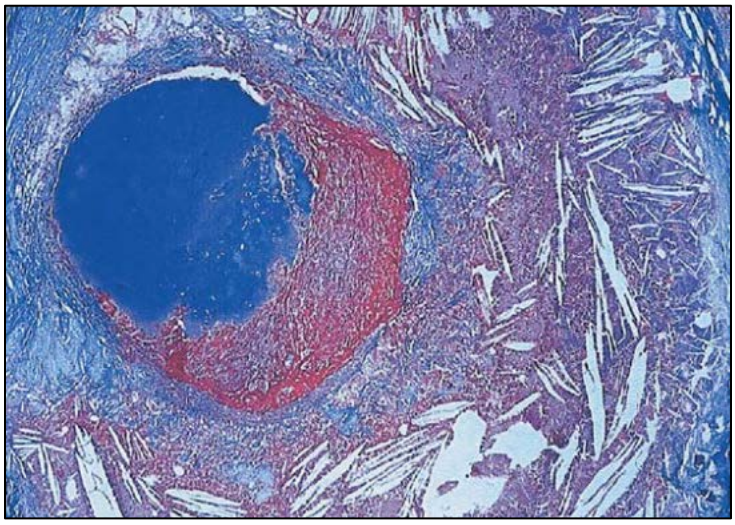

Figure 1. Lumen occluded by atherosclerotic plaque[2]. Note the ruptured portion of the plaque in the top right of the cross section. This calcium-rich rupture has the potential to initiate blood clotting in the region of the plaque and possibly occlude blood flow.

Atherosclerotic plaques experience calcification over time[2]. When atherosclerotic plaques rupture, defined as when the calcium rich core within the dense lipid outer layer of a plaque is exposed to blood flow, calcium is released into the blood stream. Calcium is a key player in the blood-clotting cascade and can promote thrombosis generation in the region of the ruptured plaque[3]. The subsequent thrombosis has the potential to embolize and lodge in small vessels within the heart and brain, among other locations. This process can result in heart attack or stroke.

Ruptured atherosclerotic plaques are responsible for 76% of all fatal heart attacks that result from coronary thrombosis worldwide[2]. Cardiovascular complications from atherosclerosis are estimated to be responsible for 50% of all deaths in western societies[1]. As atherosclerosis is one of the main contributors to heart disease, addressing it and its symptoms is one of the keys to treating heart disease and saving lives.

Section 1.2 – Where are Atherosclerotic Plaques Most Common?

Atherosclerotic plaque is most commonly found in locations of vascular branching or bifurcation[4], commonly in the carotid, coronary, femoral, and infrarenal arteries. This phenomenon has been confirmed through both medical autopsies and through non-invasive magnetic resonance imaging. The localization of atherosclerotic plaque has been found to be present in humans regardless of age, ethnic origin, or diet[5], though the severity of the plaques has been found to be dependent on these factors. An angiogram of the left coronary artery of a stroke patient is provided in figure 2. Note the narrowing at the outer walls of the coronary bifurcation caused by the atherosclerotic plaque.

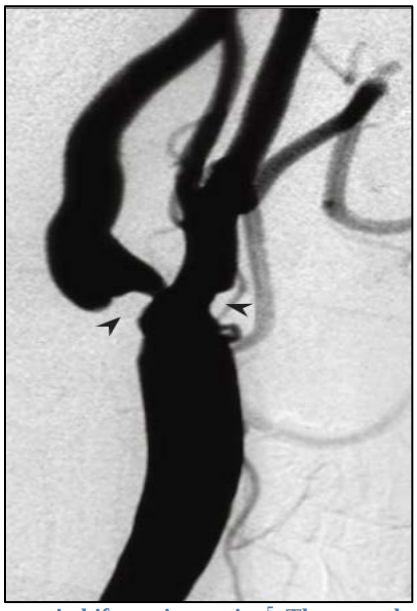

Figure 2: Angiogram of atherosclerotic artery in bifurcation region[5]. The arrowheads highlight the narrowing of the artery due to plaque formation on the outer walls where shear stress is low and flow separation is common.

A variety of theories for the causes of this localization have been proposed. The first suggests that high fluid shear stresses on the order of 400 dynes/cm^2 or greater cause vascular injury and promote generation of atherosclerotic plaque[6]. The second theory states the opposite: that low fluid shear stresses on the order of 4 dynes/cm^2 or less affect the mechanics of endothelial cells and promote atherosclerotic plaques. Multiple studies over the last three decades suggest the latter to be the likely mechanism behind

plaque deposition[5]. The low shear stress postulation will be discussed further in the next chapter of this thesis.

Section 1.3 – Current Treatment Options for Atherosclerosis

Presently, treatment of atherosclerosis is almost entirely preventative. As mentioned previously, there are several risk factors that contribute to atherosclerosis. Diets high in fat and cholesterol promote the growth of atherosclerotic plaque. Smoking and diabetes are other factors that can contribute to increased complications due to atherosclerosis. Many of the harsh chemicals contained within a cigarette have been shown to cause damage to the arterial wall and promote the buildup of low density lipoproteins (LDL) and other lipoproteins that are responsible to atherosclerosis[24]. Similar to smoking, diabetes has been shown to interfere with endothelial cell signaling pathways that help prevent LDL buildup[25]. Males are generally more susceptible to atherosclerosis, though females are just as susceptible, if not even slightly more, following menopause[7].

Atherosclerosis is mainly treated by combatting its symptoms and paired complications. For example, blood thinners can be beneficial to individuals with severe atherosclerosis by decreasing the likelihood of blood clot formation in narrow regions of the circulatory system. High blood pressure medication has also found use in treating atherosclerosis. Treating high blood pressure helps to prevent vessel swelling and damage that might accelerate atherosclerosis[1]. Until recently, there has not been an available treatment for atherosclerosis directly. Various lipid treatments now exist to help regress the size of atherosclerotic plaques. These treatments have seen successful in clinical trials in decreasing mortality rates in atherosclerosis patients[7]. However, one of the main challenges that remains is developing an effective method for drug delivery to atherosclerotic lesions. The following chapter explains how the interaction between mechanical conditions in the regions of the cardiovascular system that are prone to atherosclerotic plaque has implications for drug delivery.

Chapter 2

THE IMPACT OF FLUID MECHANICS ON ENDOTHELIAL CELL PROPERTIES

In investigating the cause of atherosclerotic plaque localization, the low shear stress hypothesis has been corroborated through a variety of studies, most notably by Ku et al. in 1985. The Ku group created a Plexiglas model of the common carotid bifurcation and used Doppler velocimetry to track velocity gradients near the vessel wall to calculate localized shear stress. Testing concluded that the outer walls of the model, where atherosclerotic plaque is most prone to formation, experienced the lowest shear stresses and flow separation in certain cases[8].

Further experimentation has found this same result. The Koskinas group constructed 3D models of swine arterial bifurcations using ultrasound techniques. Computational Fluid Dynamics (CFD) was used to determine fluid shear stress on the endothelial wall. Diabetes was induced in the swine subjects in order to promote atherosclerotic growth. A sixteen-week study found that plaque growth was highest in regions of low shear stress validated by the CFD study[9]. The following sections seek to explain how the interactions between shear stress and the endothelial cell membrane can promote or prevent atherogenic growth.

Section 2.1 – Cellular Deformation as a Result of Shear Stress

When subjected to a shear stress, endothelial cells deform as a viscoelastic liquid[10] when deformation is measured over the first 50 seconds after shear exposure. Figure 3 demonstrates the deformation over time of an endothelial cell compared to the Voigt-Maxwell model. As a shear stress is applied to a cell, the cell experiences a large initial deformation and then a gradual linear deformation as

time progresses. Oscillating shear stresses have a mitigating effect on deformation and result in deformation in multiple directions, creating a "spread" cellular morphology[8].

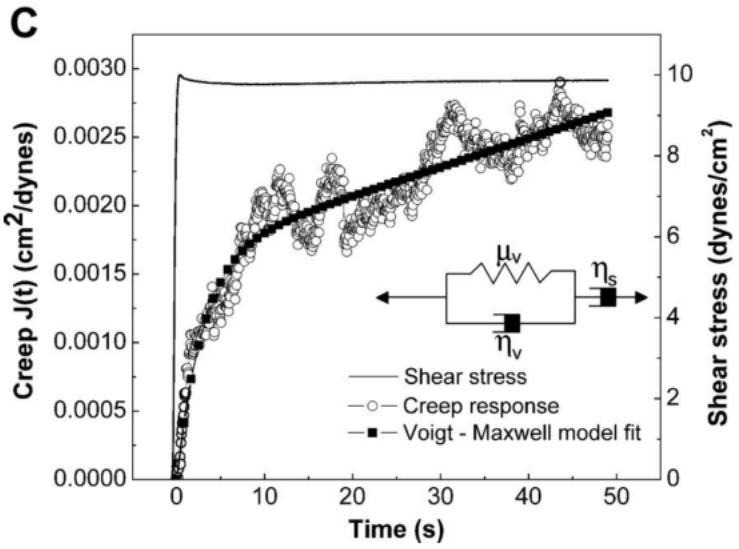

Figure 3: Creep deformation of endothelial cell in response to shear stress[10]. Deformation is fit to a Voigt-Maxwell model fit. Following a large initial deformation, the cell continues to deform as shear stress is applied over time. *Inset*: A schematic of a Voigt-Maxwell model.

New evidence suggests that shear stress leads to cell realignment (one aspect of mechanotransduction) via phosphorylation of α4 integrins on the surface of the cell membrane. Increased activation of α4 integrins leads to increased activity of the enzyme PKA[11]. PKA is necessary for actin polymerization and therefore necessary for a morphological change in cells through cytoskeletal reorganization. Phosphorylation of integrins is not only a function of intensity of force but also direction. Prolonged exposure to shear stress induces a morphological change in the direction of the applied stress[12]. Figure 4 demonstrates this morphological change over time. As more integrins are phosphorylated by the applied shear stress, the cytoskeleton reorganizes itself in the direction of the stress over time, effectively aligning the cell with the direction of the fluid flow responsible for the stress. The alignment of endothelial cells and the reorganization of the cytoskeleton have a profound impact on the mechanics of the cellular membrane.

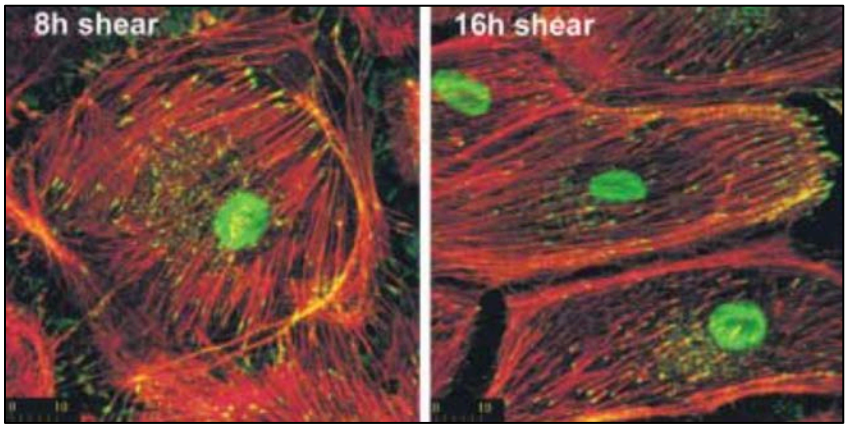

Figure 4: Alignment of endothelial cells in direction of applied shear stress over time[12]. Actomyosin filaments are stained in red and the cell nucleus in green. After 8 hours of applied shear stress, the cell is spread with actin filaments extending in all directions. After 16 hours of shear, the actin filaments are aligned in the direction of flow and the cell is considerably elongated.

Section 2.2 – Shear Stress Changes the Cell Membrane

Cytoskeletal actomyosin filaments, which can be aligned via the application of a shear stress to the cell membrane, have a profound impact on the mechanical properties of cells, particularly their stiffness. Gavara & Chadwick transfected endothelial cells with Green Fluorescent Protein (GFP) hybridized to bond with actomyosin stress fibers. The group quantified the amount and orientation of stress fibers using 20x fluorescence imaging and Matlab. Atomic Force Microscopy (AFM) was then used to measure the stiffness of the transfected cells. AFM analysis found a strong correlation between the alignment of stress fibers and the stiffness of the cells stained with GFP[13]. Factors such as cell area or thickness of stress fibers were not found to have an effect on cellular stiffness.

Section 2.3 – Measuring Cell Membrane Changes using Traction Force Microscopy

In order to migrate on a substrate, cells form connections with the substrate called focal adhesions. Cytoskeletal reorganization propels the cell in the direction of migration as the cell exerts small forces on the Extra Cellular Matrix (ECM) at focal adhesions. These forces, called Cellular Traction

Forces (CTFs), can be measured through variety of methods, chiefly Traction Force Microscopy (TFM). TFM is performed by plating cells on a gel embedded with fluorescent beads. As the cells migrate and exert traction forces, the beads are displaced within the gel. By tracking the displacement of the beads, it is possible to calculate the forces that the cell applies to the ECM[37]. TFM can create stress profiles of individual cells (Figure 5) and entire colonies of cells (Figure 6).

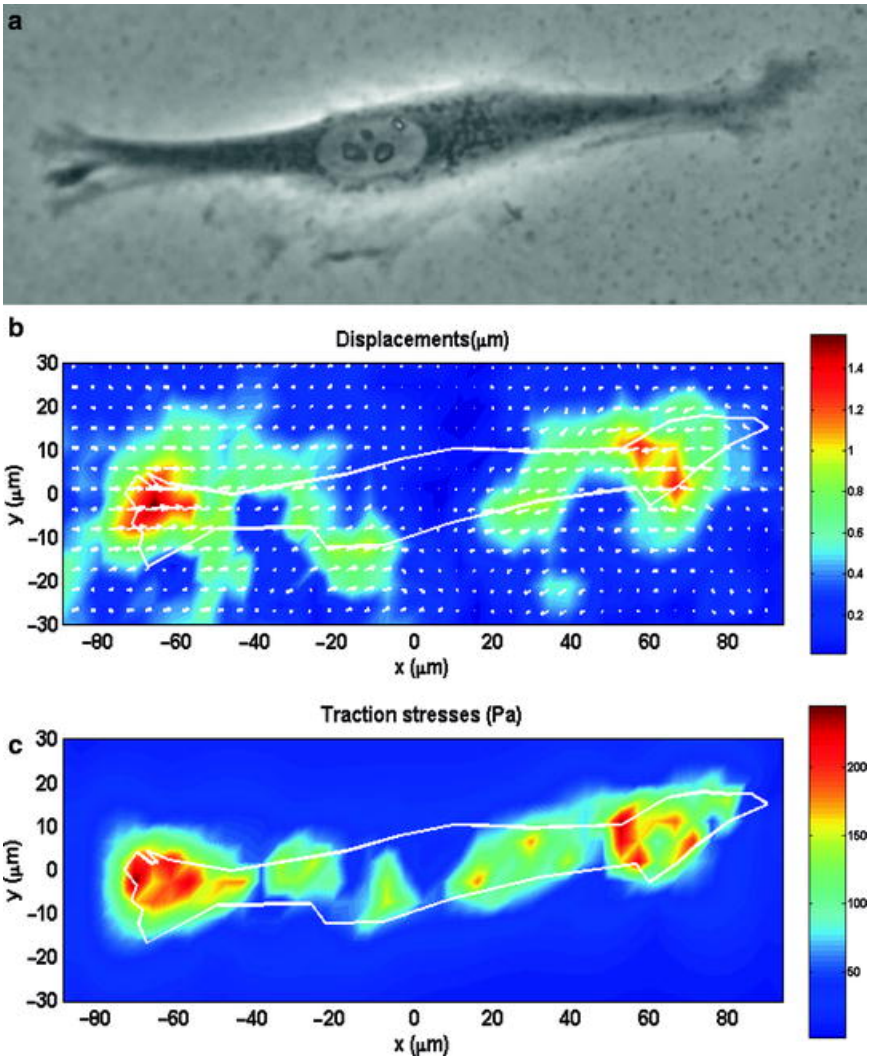

Figure 5: Stress profile of singular endothelial cell[37]. Higher forces are measured at the leading and trailing end of the cell.

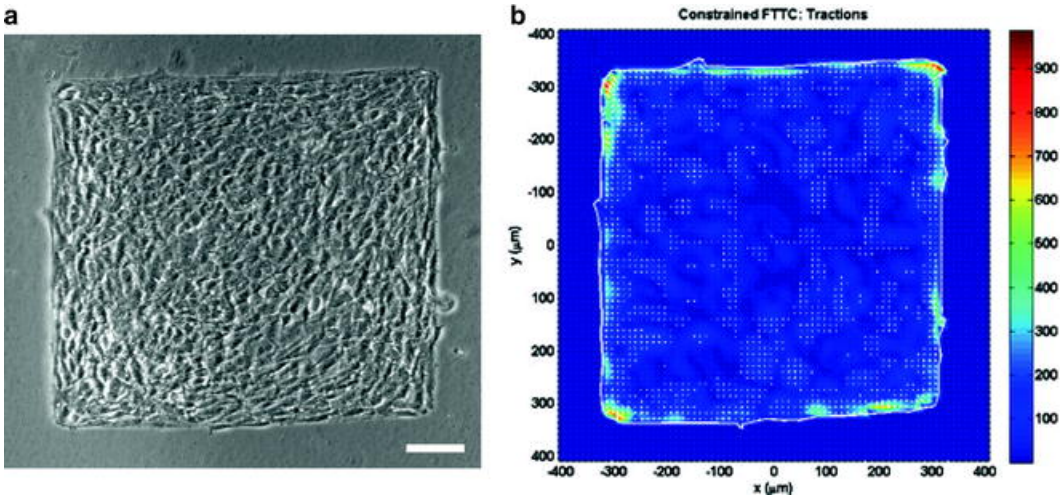

Figure 6: Stress profile for entire colony of endothelial cells[37]. Stresses are particularly low in regions where cells have achieved confluence.

Recent efforts have been made to predict the stiffness of cellular membranes through traction force measurements. Zhang et al. derived a method to measure the Young's modulus of HCT-8 epithelial cells through traction force profiles resulting from TFM[38]. This advancement creates the possibility to measure the stiffness profiles of individual cells and cell colonies without using methods such as AFM that require physical contact with the cells.

In summary, shear stresses deform and align endothelial cells in the direction of flow. This alignment and subsequent cytoskeletal reorganization of stress fibers has a profound impact on the stiffness of cells. Traction Force Microscopy is one method that can potentially be used to measure the stiffness of cells under different shear stresses and flow conditions. The following section explains the significance of cellular stiffness in the pathology of atherosclerosis and the potential for new treatment.

Chapter 3

NANOPARTICLES: THE FUTURE OF ATHEROSCLEROSIS TREATMENT

Nanoparticles are biodegradable polymers on the order of 100 nanometers or less that are considered one of the most promising avenues for disease treatment and prevention. Nanoparticles can be formulated with the goal of encapsulating or attaching drugs. In this manner, nanoparticles can serve as an advanced method of drug delivery[14]. One of the main advantages of nanoparticles is that they can be modified to serve specific roles in drug delivery. For example, the surfaces of nanoparticles can be functionalized to interact with certain molecules, such as adhesion proteins on the cell membrane. Nanoparticles can also be tuned to release a controlled concentration of drugs over a period of time[15]. One of the current challenges to treating atherosclerosis is developing effective methods to target diseased cells with treatment. Nanoparticles may be the answer to this challenge. In order to understand how and why this is the case, one must first understand how nanoparticles interact with and enter cells.

Section 3.1 – Cellular Endocytosis of Nanoparticles

Nanoparticles (NPs) first interact with the cell through an adhesion with various ligands on the surface of the cellular membrane. Depending on the strength of the interaction, the adhesion force may reach a threshold where the endocytosis process can take place. The first step of the endocytosis process is the “wrapping” phase, where a portion of the cellular membrane bends away from its curved intrinsic shape and starts to wrap around the surface of the NP[16]. This phenomenon is illustrated in figure 7. The wrapping phase is of interest because properties that are modified by shear stress in endothelial cells are key players in the mechanics of endocytosis.

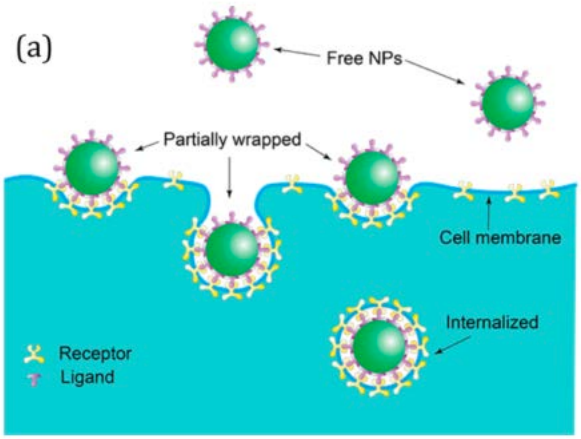

Figure 7: Membrane wrapping and internalization of a nanoparticle[16]. Particles are internalized once the membrane wraps entirely around the particle. Increased stiffness in the cell membrane inhibits this process.

Huang et al. explored the impacts of cellular membrane stiffness on the amount of nanoparticles that are endocytosed by endothelial cells. Membrane stiffness was modified by culturing cells on substrates of varying stiffnesses. Fluorescent nanoparticles were then introduced to the cell media and the cellular uptake of nanoparticles was quantified over 12 hours by measuring the intensity of the fluorescence within the cells. Cells that were cultured on stiffer substances and thus had stiffer membranes had lower NP uptake than cells cultured on soft substrates[17]. This phenomenon may be explained by the wrapping phase. When cellular membranes are especially stiff, due to high surface tension or other factors, they do not bend as easily. This difficulty in bending can inhibit the wrapping phase and prevent NP endocytosis.

Particles can also travel through or behind the endothelial cell through “leaky junctions.” Cells are joined through tight junctions and use these pathways to communicate. “Leaky junctions” are less secure tight junctions, often exhibited by cells undergoing mitosis or apoptosis. More recently, leaky junctions have been observed in cells that experience low shear and disturbed flow[18]. Cells in regions that experience the above conditions may have an improved permeability to NPs and other particles.

Section 3.2 – The Enhanced Permeability and Retention Effect

Nanoparticles are commonly explored in cancer treatment efforts because of a phenomenon called the Enhanced Permeability and Retention (EPR) effect. The EPR effect describes the enhanced perfusion of macromolecules in the bloodstream into tumor tissue. This phenomenon is due to a variety of factors, including poorly aligned endothelial cells, misshapen blood vessels, and poor lymphatic drainage[19]. These factors allow for the increased infiltration and retention of nanoparticles in tumor tissue, lending NP treatment to be a very effective option.

Many of the factors that contribute to the EPR effect are present in regions of common atherosclerotic plaque buildup[26]. The endothelial cells are particularly poorly aligned and the smooth muscle layer underneath the endothelial cells is often damaged or disorganized. These characteristics suggest that NP treatment also has particularly promising merits in treatment of atherosclerosis.

Section 3.3 – Opportunities for Atherosclerosis Treatment through Nanomedicine

Utilizing the EPR effect for nanoparticle delivery to atherosclerotic cells is just one of the methods being explored for atherosclerosis treatment. Nanoparticles can be functionalized by attaching proteins to their surface in order to direct them towards specific targets. For example, by functionalizing NPs with adhesion molecule VCAM1, NPs are much more likely to bind with endothelial cells that express the receptor for that specific ligand. The NPs can then be internalized by the cell and release the encapsulated treatment[26]. Though functionalizing NPs can have a strong impact on whether or not they are internalized by cells, NP trajectory to diseased sites is still largely dependent on vascular permeability and the EPR effect at the site of interest[27].

One factor that has been shown to aid the delivery of NPs to atherosclerotic sites is red blood cell (RBC) margination, in some cases increasing NP delivery by as much as 50%[35]. Red blood cell margination is the process in which nanoparticles or other macromolecules in the blood stream migrate

towards the vessel walls. RBCs are pushed towards the center of blood vessels through interactions with the vessel wall called lift forces. Consequently, smaller particles are marginated to the outer edge of blood vessels. The range of particle margination is a strong function of particle size and shape. Particles that are spherical in shape with diameters in the 100 to 200 nm range tend to migrate to regions of the vessel cross-sectional area that are more plasma-dense such as near the vessel wall. Particles in the micron range have been shown to have an even stronger tendency to move towards the vessel wall, although particle sizes in the micron range may have difficulty entering into capillaries[28]. Increased transport of nanoparticles towards the vessel wall via red blood cell margination increases the adhesion efficiency of nanoparticles and thus increases their effectiveness as a treatment method[36].

Section 3.4 – Fluid Flow Impacts Mass Transport Properties of Cells

John Tarbell determined that certain flow conditions exist where fluid mechanics have a strong effect on mass transport properties of cells. This interaction can be quantified using two dimensionless parameters: the Sherwood number (dimensionless mass transfer coefficient) and the Damkholer number (dimensionless reaction rate coefficient). The Sherwood number is the ratio of the convective mass transfer rate to the diffusion rate of a species. Convective mass transfer is the transport of a species that is driven by a fluid flow, while diffusive mass transfer is the transport of a species due to a concentration gradient. High Sherwood numbers indicate a process where mass transfer is primarily driven by a fluid flow, while low Sherwood numbers indicate a process where mass transfer is driven by a concentration gradient. The Sherwood number can be calculated as follows:

$$Sh = \frac{k_L d}{D} \quad \textbf{(1)}$$

where k_L is the mass transport coefficient of the solute in blood, d is the diameter of the vessel, and D is diffusion coefficient of the species in blood[31].

The Damkohler number is the ratio of the reaction rate of a species and the convective mass transport rate of a species. Reaction rate is the transport of a species that binds to a surface and undergoes a reaction that transports it across the surface. High Damkholer numbers indicate a process where mass transfer is primarily driven by reactions, while low Damkholer numbers indicate a process where mass transfer is primarily driven by fluid flow. There are two variations of the Damkholer number that are of interest when characterizing the interaction between fluid flow and mass transport. The first Damkholer number of interest is the Damkholer number for reactive surfaces. This variation of the Damkholer number is specific to molecules that must bind to the cellular membrane in order to be transported across such as ATP. The reactive surface Damkholer number can be calculated as follows:

$$Da_r = \frac{k_r d}{D} \quad \textbf{(2)}$$

where k_r is the 1st order reaction rate constant for consumption of the solute at the endothelial surface[31]. The reactive surface Damkholer number is relevant for drug delivery solutions that require reactions at the surface of endothelial cell membranes, such as with a hybridized nanoparticle.

The next variation of the Damkholer number that is of interest is the permeable surface model. The permeable surface model is specific to larger molecules that can enter cells through passive channels and junctions. The permeable surface Damkhloer number can be calculated as follows:

$$Da_e = \frac{P_e d}{D} \quad \textbf{(3)}$$

where P_e is the permeability coefficient for the surface[31]. The permeable surface Damkhloer number is relevant for drug delivery solutions where particles enter cells through passive methods such as through leaky junctions. There is a third Damkholer number that exists, the reactive wall Damkholer number, that pertains to the transport of extremely small molecules, such as oxygen, across the cell membrane. Since molecules that small are not relevant to drug delivery to atherosclerotic plaque, the reactive wall Damkholer model will not be discussed further.

In conditions where Da << Sh, the process is said to be “reaction limited,” which means that the rate at which the solute can react with the cellular membrane is the primary mediator of mass transport

across the cell membrane. In conditions where Da >> Sh, the process is said to be “transport limited,” meaning that the fluid flow around the cell is the primary mediator of mass transport across the cell membrane.

Measurements of Sherwood and Damkholer numbers in relevant regions help to bolster the hypothesis that fluid dynamics and mass transport are heavily intertwined at the interface between blood and endothelial cells. Perktold et al. utilized computational modeling of particle transport in pulsatile flow for an anatomically realistic 3D carotid artery bifurcation. Particle transport was measured in the outer walls of the model that experienced flow separation and recirculation. The Sherwood number predicted by the model was almost exactly zero[32]. In rabbit aortas, Truskey et al. measured endothelial permeability to LDL in order to calculate the Damkholer number for LDL. The Truskey group found that the Damkhloer number for LDL in regions of turbulent flow was around 0.02, but was roughly 1 in regions where endothelial cells were undergoing mitosis[33]. Since cells undergoing mitosis often exhibit leaky junctions, similar to endothelial cells in flow recirculation regions[18], it is reasonable to assume that the Damkholer number for LDL in flow recirculation regions is relatively close to the measured value around cells undergoing mitosis[34], although no direct effort to measure the Damkholer number of LDL in recirculatory regions has been made as of yet.

Because the measured Sherwood number in the bifurcated carotid artery is several magnitudes smaller than the measured Damkholer number for LDL in comparable conditions, a strong argument can be made that the recirculating flow conditions in the carotid bifurcation are a strong determinant of the uptake and deposition of LDL that leads to atherosclerotic plaque genesis.

Section 3.5 – Bridging the Gap Between Atherosclerosis Pathology and Treatment

To review, atherosclerosis is a progressive disease of the arteries where low-density lipoproteins (LDLs) are deposited in the vasculature over time to form plaques. The plaques can result in a variety of complications including heart attacks and stroke. Plaques generally form in the region of bifurcations of arteries. The leading theory behind the localization of plaques is that the main contributor is the low shear stress and flow separation in those regions.

Endothelial cells deform in response to shear stresses. The cytoskeleton reorganizes and cells align with the direction of the flow. Aligned cells, which can be found in regions where flow is linear, are very stiff in comparison to spread cells, which can be found in bifurcated regions of the vasculature where flow recirculation is common and shear stress is low. Spread cells have membranes that are relatively soft and permeable, meaning it is easier for macromolecules to enter the cell through endocytosis or leaky junctions.

The enhanced permeability of cells in recirculation regions is likely the key contributing factor to the localization of plaque growth and is highly proatherogenic. However, the same factors that make endothelial cells susceptible to LDL deposition may also provide an avenue for treatment using nanoparticles. In order to test this hypothesis, it is necessary to construct a flow chamber to mimic characteristics of bifurcation regions to understand if cells in those regions will uptake more NPs than cells in aligned flow regions.

Chapter 4

METHODS

Though several groups have validated the individual biophysical theories behind this work, there has yet to be a comprehensive investigation into the intersectionality between cellular mechanics, fluid mechanics, and mass transport for atherosclerosis treatment applications. This chapter will discuss in detail the setup for an investigation into the effects of fluid recirculation on cellular uptake of nanoparticles. Both computational modeling and experimental testing with a physiologically accurate flow chamber will be discussed.

The desired flow chamber requires four key attributes: recirculation in the flow, the inclusion of porous media, cells seeded normally to the direction of flow recirculation, and the ability to image in real time in high resolution. Computational modeling in Comsol Multiphysics software was used to drive the design of the flow chamber. The flow chamber was subsequently manufactured by modifying an existing Bioptechs FCS2 chamber in the Mechanobiology Laboratory.

Section 4.1 – Computational Modeling in Comsol

Comsol Multiphysics software is a cross-disciplinary finite element analysis and physics simulation software. Comsol is a useful tool for the early design stages of the flow chamber because it allows for design iteration without the time or cost of building a physical model. Comsol modeling also is useful in making predictions about how the physical flow chamber might perform. A sound computational model can be helpful in determining whether the physical flow chamber is functioning as is intended.

Section 4.1.1 – Model Geometry

A two dimensional flow chamber was generated in Comsol to simulate the flow dynamics and is pictured in Figure 6. The model was designed specifically to produce flow recirculation. Expansion ratio (ER) is defined as the height of an expanded region of flow over a contracted region. For example, and expansion ratio of 3 could be characteristic of a backwards facing step flow chamber with an inlet 1 mm high and an expanded region 3 mm high. Poole et al. determined that ERs greater than or equal to 1.25 are necessary to induce flow recirculation[20]. The Comsol model has an ER of 2.43, which is more than sufficient to induce a large flow recirculation region. The model in figure 8 is horizontally bisected. The top region is an open chamber for fluid flow. The bottom region is a porous matrix that represents the edge of a cell membrane. The whole chamber spans 1 mm vertically. This is done to accommodate for space restrictions associated with the microscope that will be used for imaging.

Figure 8: Geometry of Comsol model. Flow travels from left to right. The step shape induces a large flow recirculation zone shortly after the left expansion.

Section 4.1.2 – Material Properties

The material properties for the fluid in the upper section were defined to be the properties of water – a density of 1000 kg/m^3 and a viscosity of 1 centipoise. For preliminary runs with the physical flow chamber, water will be used; however, blood analogs may be used further down the line. For the time being, simulating with water is appropriate. The particles released into the flow were given a density of 1300 kg/m^3 and a diameter of 100 nm.

The lower half of the model is given different properties. The lower half of the model shares the properties of a polyacrylimed gel (PAG) used for Traction Force Microscopy applications[37]. Polyacrylimide gel is suitable for this application because it provides substantial resistance to fluid and will help drive interstitial flow through the cultured endothelial cells. The gel has a permeability of $27x10^{-16}$ m^2 and a porosity of 0.33[39]. The Polyacrylimide gel selected for this experiment has a Young's modulus of 20 kPa and a Poisson's ratio of 0.48[37].

Section 4.1.3 – Model Physics

Steady state laminar flow is evaluated in the top region. In the laminar flow simulation, the Navier-Stokes equation is solved for the velocity of the fluid at any point. Laminar flow is described by the modified incompressible Navier-Stokes equation:

$$\rho(u \cdot \nabla)u = \nabla \cdot [-p + \mu(\nabla u + (\nabla u)^T)] + F \quad \textbf{(4)}$$

where ρ is the fluid density, u is the fluid velocity, ∇ is the gradient operator, p is the pressure, and F is the body force applied to the fluid. Equation **(4)** can be rewritten as:

$$\rho(u \cdot \nabla)u = -\nabla p + \rho g + \mu \nabla^2 u \quad \textbf{(5)}$$

where g is the acceleration due to gravity. The Navier-Stokes Equation states that the momentum of a fluid must be conserved.

The upper region is also subject to the continuity equation. The continuity equation states:

$$\rho \nabla \cdot u = 0 \quad \textbf{(6)}$$

which means that the mass of a fluid must be conserved.

The Brinkman Equations are evaluated in the bottom region of the model. The Brinkman Equations are used to compute the fluid velocity and pressure gradients of single phase, laminar flow through porous media at any location. The Brinkman Equations are as follows:

$$0 = \nabla \cdot \left[-p + \mu \frac{1}{\varepsilon_p}(\nabla u + (\nabla u)^T)\right] - \left(\mu \kappa^{-1} + \beta_F |u| + \frac{Q_{br}}{{\varepsilon_p}^2}\right) u + F \quad \textbf{(7)}$$

where ε_p is the porosity of the porous medium, κ is the permeability of the porous media, and Q_{br} is equivalent to $\rho \nabla \cdot u$. The Brinkman equations can be simplified to the form:

$$\langle \nabla p \rangle = -\frac{\mu}{\kappa} u + \mu_e \nabla^2 \langle u \rangle \quad \textbf{(8)}$$

where μ_e is the effective viscosity, or the parameter that equates the shear stress boundary condition at the fluid-porous matrix interface.

Particle tracing for fluid flow is solved for in the top region in a time dependent study. Particle tracing computes the motion of particles in a fluid. The Particle tracing equations are as follows:

$$\frac{d(m_p u)}{dt} = F_t \quad \textbf{(9)}$$

where m_p is the mass of the particle and F_t is the applied force that drives the motion of the particles. In this case, the applied forces are drag force and Brownian force.

Drag force is a force applied to an object by a fluid that acts opposite to the object's direction. The drag force equation is as follows:

$$F_D = \frac{1}{\tau_p} m_p (u - v) \quad \textbf{(10)}$$

where v is the velocity of the particle in the y direction and τ_p is the drag coefficient. The drag coefficient is defined as:

$$\tau_p = \frac{\rho_p {d_p}^2}{18\mu} \quad \textbf{(11)}$$

where ρ_p is the particle density and d_p is the particle diameter.

Brownian force results in the diffusion of particles suspended in a fluid away from the fluid's streamlines. It is defined as:

$$F_b = \zeta \sqrt{\frac{12\pi k_b \mu T r_b}{\Delta t}} \quad \textbf{(12)}$$

where ζ is the friction coefficient, k_b is the Boltzmann's constant, T is temperature, r_b is the radius of the particle, and t is time.

Figure 9 labels the two regions of the Comsol model. Table 1 displays the applicable physics and material properties to each region.

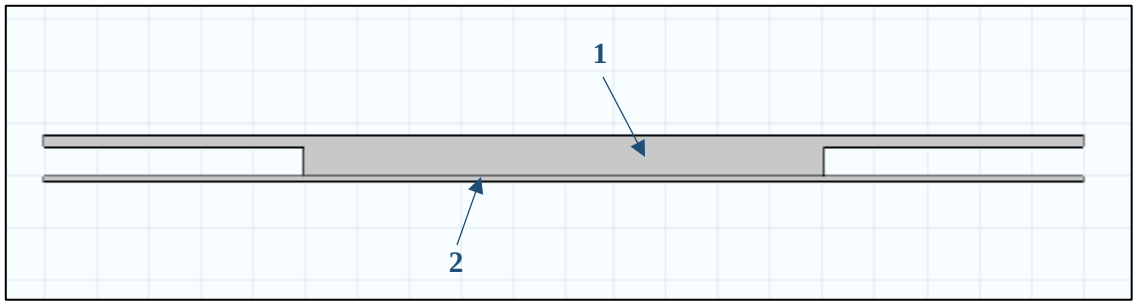

Figure 9: Labeling of two Comsol model regions. Laminar flow and particle tracing is studied in the region labeled 1. Flow through porous media (Brinkman equations) is studied in the region labeled 2.

Table 1: Material Properties and Relevant Physics by Model Region

Region #	Material Properties	Relevant Physics
Region 1	ρ_f = 1000 kg/m^3	Navier-Stokes Equation **(4)**
	μ = 1 cP	Continuity Equation **(6)**
	ρ_p = 1300 kg/m^3	Particle Tracing Equation **(9)**
	d_p = 50 nm	Drag Force **(10)**
		Brownian Force **(12)**
Region 2	κ = 27e-16 m^2	Brinkman Equations **(7)**
	ε_p = 0.33	
	Y = 20 kPa	

Section 4.1.4 – Comsol Model Boundary Conditions

Various boundary conditions are applied to the chamber geometry to solve the relevant governing equations. The laminar flow study has four boundary conditions: two wall conditions, an inlet, and an outlet. The first wall condition is the no-slip condition, which states that the velocity tensor of a particle at a wall is equal to the velocity of the wall, in this case zero. The second wall condition is a "leaking wall," which states that the boundary is essentially completely permeable and that streamlines can freely pass through the wall. One wall is selected as the flow inlet, where the inlet velocity is specified to be 0.4 m/s. The inlet velocity was derived from work performed by Sharif et al. where echocardiography was used to determine the mean flow velocity in the left anterior descending coronary artery[23]. Since the left coronary artery bifurcation is both one of the most common and most problematic areas for atherosclerotic plaque[1], it is suitable for this application. The outlet for the laminar flow was set to a pressure of 0 Pa with suppressed backflow. The upper chamber was given initial values of 0 m/s for velocity and 0 Pa for pressure.

Like the laminar flow study, the Brinkman equations study was also given initial conditions of 0 m/s fluid velocity and 0 Pa of pressure. The no slip condition was also applied to most of the model, as was the leaking wall condition on the interface between the free and porous media.

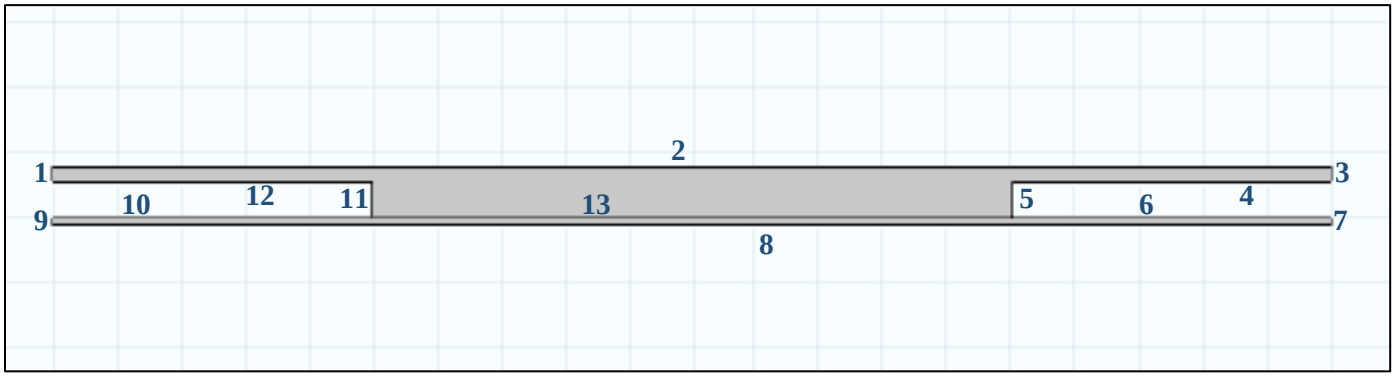

Figure 10: Labeling of model boundaries. Boundaries are numbered in the clockwise direction starting at the flow inlet. The condition applied to each boundary can be found in Table 2

The particle tracing study also has two wall conditions, an inlet, and an outlet condition. The majority of the model is set to the wall condition of "bounce," which specifies that particles that particles are rebounded off the surface with equivalent velocity and complementary angle. The next wall condition is set to "freeze," which states that when a particle contacts a wall, its position is frozen but it retains its velocity. This represents the cellular uptake of a particle. For the inlet of the particles, 500 particles are released every 0.1 s for 1 s. The velocity of the particles is determined by the streamlines from the laminar flow study. At the outlet, particles are set to the "disappear" condition where they are removed from the model entirely upon contact. Figure 10 labels all fifteen of the boundaries. Table 2 explains the condition at each boundary and the relevant governing equation.

Table 2: Conditions Applied to Each Boundary

Boundary Condition	Relevant Governing Equation	Boundaries Applied
Fluid Inlet	$u_{fluid} = 0.4$ m/s	1
Fluid Outlet	$p_0 = 0$ Pa	3
No Slip Condition	$u_{fluid} = 0$ m/s	2, 4, 5, 6, 7, 8, 9, 10, 11, 12
Leaking Wall		13
Particle Inlet	$u_{particle} = u_{fluid}$	1
Disappear		3
Bounce	$u_{particle} = \|u_{particle}\|\tan(180-\theta)$	2, 4, 5, 11, 12
Freeze	$v_{particle} = v_{particle}$	13

Section 4.2 – Flow Chamber Manufacturing Process

This section details the design and manufacturing process for the proposed flow chamber. The general design of the flow chamber, as well as the modifications to the existing Bioptechs FCS2 flow chamber, the porous media polymerization, and silicon gasket manufacturing process will be explained.

An exploded view of the flow chamber is shown in Figure 11. Each component is labeled and its function is discussed in the subsequent section.

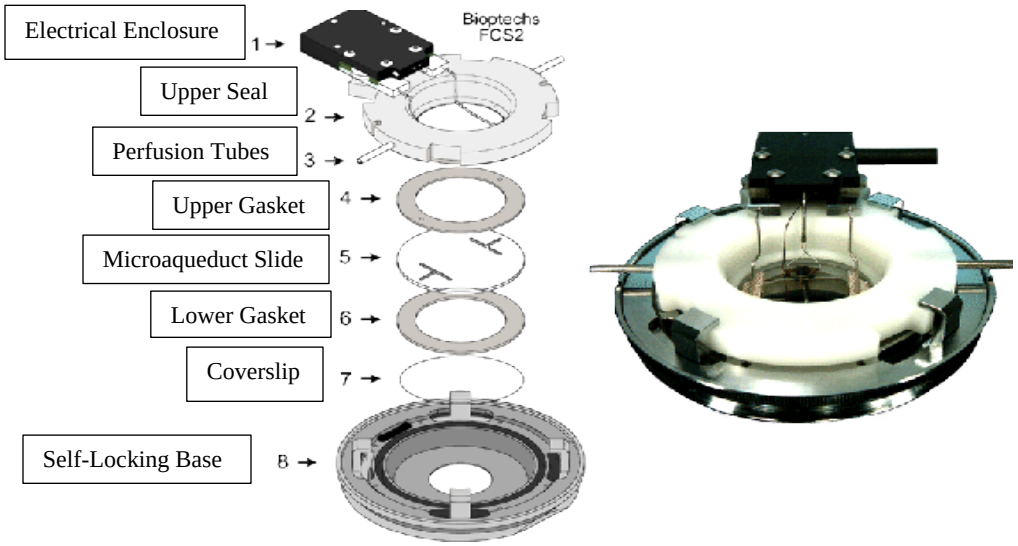

Figure 11: FCS2 Flow Chamber[30]. *Left:* Exploded view of FCS2 with all 8 components labeled. *Right:* Assembled flow chamber.

The main flow chamber is comprised of the microaqueduct slide, lower gasket, and coverslip. The lower gasket gives the chamber the desired geometry by creating an empty volume for fluid flow. The lower gasket is enclosed by the coverslip, which comes in contact with the microscope objective, and the microaqueduct slide, where flow enters. The microaqueduct slide is maintained at 37 ºC by the electrical enclosure in order to keep the endothelial cells at body temperature. Flow enters and exits the flow chamber via the perfusion tubes. The upper gasket and upper seal complete the flow chamber and prevent leaks.

A polyacrylamide gel (PAG) suitable for Traction Force Microscopy was selected for use as the porous media for this experiment. Polyacrylamide gel is appropriate for this application because of its strong biocompatibility characteristics and the ability to modulate the stiffness of the gel. The gel was polymerized in the method described in Appendix B. The protocol outlined in Appendix B results in gel that is roughly 100 μm thick, thin enough to image through using DIC and fluorescence microscopy. The PAG is treated with fibronectin to encourage focal adhesion formation between the endothelial cells and the gel.

The lower gasket of the flow chamber was manufactured using two techniques. First, silicon gaskets (High-Purity High Temperature Silicone Rubber, McMaster-Carr) were layered upon one another to create the open chamber for flow. Gaskets were cut to geometry using high energy laser-cutting techniques. The geometry of each layer can be found in Appendix A. The completed gaskets are shown in Figure 12.

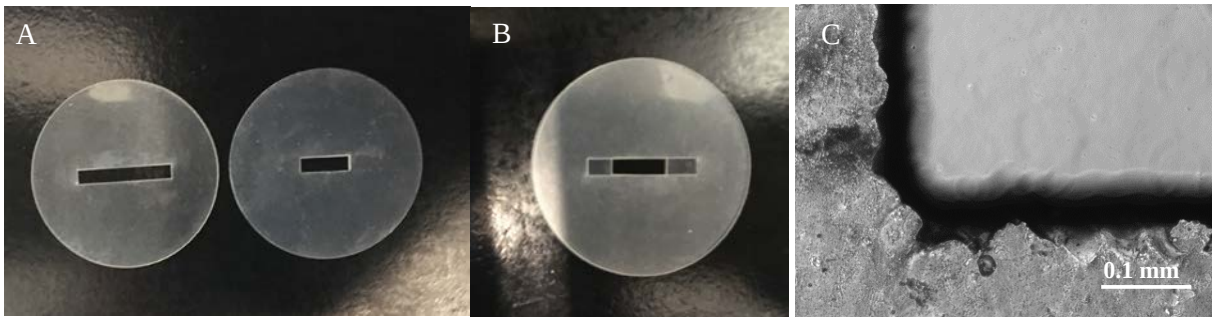

Figure 12: Laser cut gaskets for flow chamber geometry. A: Geometry of thinner top gasket (left) and thicker bottom gasket (right). B: Assembled gaskets. C: Phase microscopy image of laser cut gasket at 20X magnification. The hole in the upper right is cut to a high resolution with little debris.

Additive manufacturing techniques were also explored for manufacturing the gasket. In a previous collaboration between the Mechanobiology Laboratory and Jiayue Huang of Shanghai Jao Tong University, gaskets were successfully printed using an Objet500 Connex3 printer (Stratasys, Eden Prarie, MN) and TangoPlus material (Stratasys). The completed gasket, used for another flow chamber application, is shown in Figure 13. Access to an Objet printer capable of printing with TangoPlus is not available at Penn State, so 3D printers home to the Biomedical Engineering Department were investigated. Gaskets were printed using a LulzBot TAZ 6 3D printer (Aleph Objects, Inc., Loveland, CO). The CAD model for the gasket can be viewed in Appendix A. NinjaFlex (NinjaTek, Manheim, PA), a thermoplastic polyurethane material, was selected as the filament due to its superior flexibility, elongation capacity of over 600%, and Shore Hardness value of 85A[35]. The softness and flexibility of NinjaFlex allow it to be compressed into a tight seal between the cover slip and microaqueduct slide.

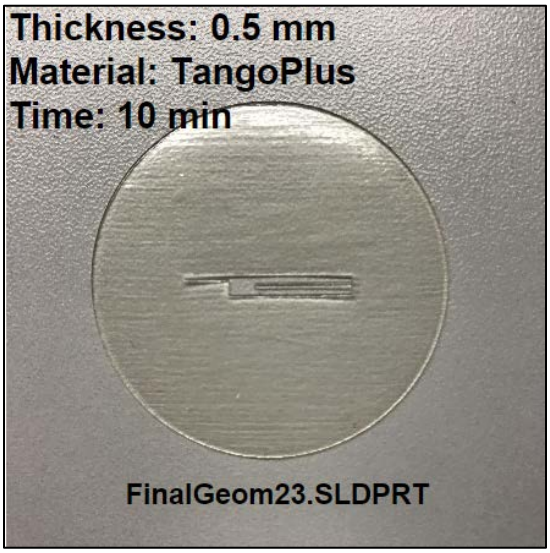

Figure 13: Gasket 3D printed using Objet500 Connex3 printer and TangoPlus material. The flexibility of the material and high resolution of the printer result in a quick to manufacture and effective solution.

Section 4.3 – Experimental Setup

In this section, the process for assembling the necessary components to run the experiment is outlined in detail. The order in which the experimental components are assembled, especially when assembling the flow loop and flow chamber, is extremely crucial and should be followed carefully.

Section 4.3.1 – Culturing Endothelial Cells

Culture Human Aortic Endothelial Cells (HAECs) in 75 cm^2 Cell Culture Flasks (Corning Incorporated, Corning, NY) with Gibco DMEM (Thermofisher Scientific, Waltham, MA) in a CO_2 controlled incubator set to 37 ºC. Autoclave the FCS2 chamber coverslips, then treat the FCS2 chamber coverslips with Fibronectin, and transfer the endothelial cells to the Fibronectin-treated coverslips placed in cell culture dishes. Continue to incubate the cells on the coverslips on DMEM until the cells form a confluent layer.

Section 4.3.2 – Creating the Nanoparticle Solution

Prepare 100 mL of endothelial cell media by mixing 100 mL of DMEM with 595.74 mg (25 μM) of HEPES Buffer (Sigma-Aldrich, Burlington, MA) in order to maintain the pH of the media in the presence of CO_2. Add 100 μL of 100 nm yellow-green fluorescent beads (Thermofisher Scientific). Under a sterile laminar flow hood, use a 10 mL syringe (Becton-Dickinson, Franklin Lakes, NJ) to pass the media through a 0.2 μm micropore filter (Corning) in order to remove any contamination.

Section 4.3.3 – Calibrating the Peristaltic Pump

The Computational model uses an inlet flow velocity of 40 cm/s in order to match the flow velocity the left anterior descending coronary artery. In order to compare the results between the computational model and the flow chamber, this velocity must be matched. Since the inlet area is 0.0075 cm^2, a flow rate of 0.3 mL/s is required. The flow rate of the Masterflex L/s Model 77200-60 Peristaltic Pump (Masterflex, Gelsenkirchen, Germany) used in this experiment is set using a dial that does not explicitly label the flow rate (Figure 14). Therefore, the peristaltic pump requires calibration in order to determine the relationship between the dial setting and flow rate. The pump was run at each knob setting for 60 s and the amount of fluid pumped into an empty test tube in that time span was collected and weighed. The mass flow rate for each knob setting was calculated and then converted to a volumetric flow rate. It was determined that setting the knob just below the number 1 was sufficient to achieve a flow rate of 0.3 mL/s.

Figure 14: Control panel of peristaltic pump. Flow rate is set using an unlabeled knob.

Section 4.3.4 – Preparing the Microscope

The experiment is performed using an Olympus IX71 Microscope (Olympus Corporation, Shinjuku, Tokyo, Japan). Consult Figure 16 for microscope layout. Turn on the PCO High Speed Camera (PCO Tech, Romulus, MI) and Fluorescent Burner (Olympus Corporation). Open shutters 2 and 3 on the Four Channel Shutter Driver (Uniblitz Shutter Systems). Screw the 10X fluorescence objective (Olympus Corporation) onto the microscope. Ensure the microscope is set to setting 4 – FITC. Plug the FCS2 Electrical Enclosure into the Chamber System Controller (Bioptechs) and set the temperature to 37 ºC. Screw the black FCS2 base onto the microscope stage to ensure the flow chamber will not shift during the experiment. Place the Aquasonic Sonicating Water Bath (VWR International, Radnor, PA) next to the microscope. Set the water bath to 37 ºC and verify the temperature with a thermometer. Open up the

Camware Software (PCO Tech) on the desktop. Place a 2mm Micrometer Slide (Leica Microsystems, Wetzlar Germany) onto the microscope and focus on the scale bar. Capture an image of the scale bar for later use.

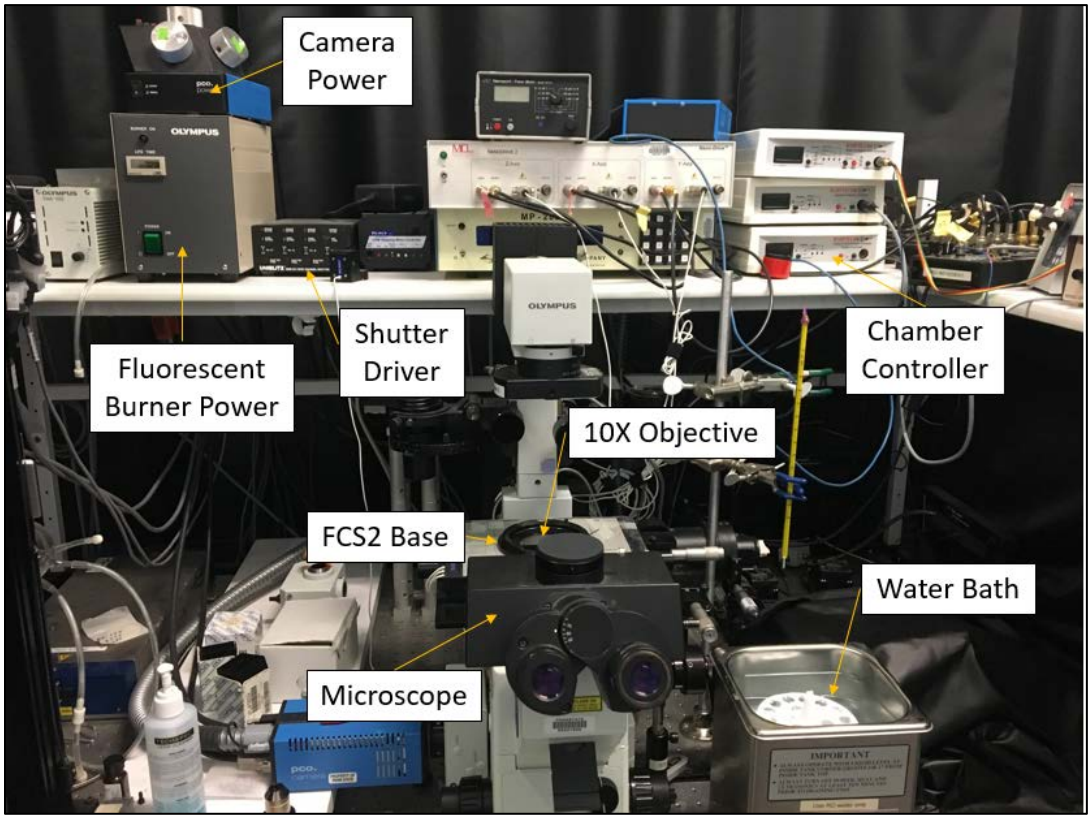

Figure 15: Microscope layout. Each component referenced in Section 4.3.4 is labeled appropriately in this figure.

Section 4.3.5 – Assembling the Reservoir, Flow Loop, and Flow Chamber

Each component necessary for assembling the flow chamber is listed in Table 3. Table 3 indicates where each component is used and whether or not it needs to be autoclaved. Before placing tubing in the autoclave, flush all tubing with 70% ethanol to clear out any debris.

Table 3: Flow Loop Components Delineated by Subsystem and Sterility

Component	Subsystem of Flow Loop	Autoclaved?
250 mL Flask	Reservoir	Yes
Cell media		
Flask stopper	Reservoir	Yes
Three 1 mL diameter glass pipets	Reservoir	No
Triangular file	Reservoir	No
Red flask ring weights	Reservoir	No
Styrofoam lid	Reservoir	No
Three 50 cm lengths of PharMed tubing	Loop	Yes
One 10 cm length of PharMed tubing	Reservoir	Yes
0.2 µm micropore filter	Reservoir	No
Peristaltic pump	Loop	No
250 mL beaker	Loop	No
Forceps	Chamber	Yes
Perfusion tube assembly	Chamber	Yes
Upper gasket	Chamber	Yes
Lower thin gasket	Chamber	Yes
Lower thick gasket	Chamber	Yes
Coverslip with cells	Chamber	Yes

After autoclaving the necessary components, spray each component in Table 3 with 70% ethanol and bring it under a sterile laminar flow hood. With the 1 mL diameter glass pipets (VWR International) still in the packaging, use a triangular file to score two of the glass pipets 15 cm from the bottom, and one of the glass pipets 5 cm from the bottom. Snap the pipets at the scoring mark and remove them from their packaging. Pour the 100 mL of media into the 250 mL flask. Push each of the pipets through the holes in the flask stopper. Place the flask stopper into the opening of the flask, ensuring the opening is sealed and the tips of the 10 cm pipets are submerged in the media. Slide the red flask ring weights into place over the flask and place the Styrofoam lid on top of the weights. Connect one 50 cm length of PharMed tubing (Masterflex) to each of the open ends of the 10 cm pipets. Attach the 10 cm length of PharMed tubing to the 5 cm glass pipet. Place the thin end of the 0.2 µm micropore filter into the open end of the 10 cm PharMed tubing. The completed reservoir should look like the reservoir displayed in Figure 16.

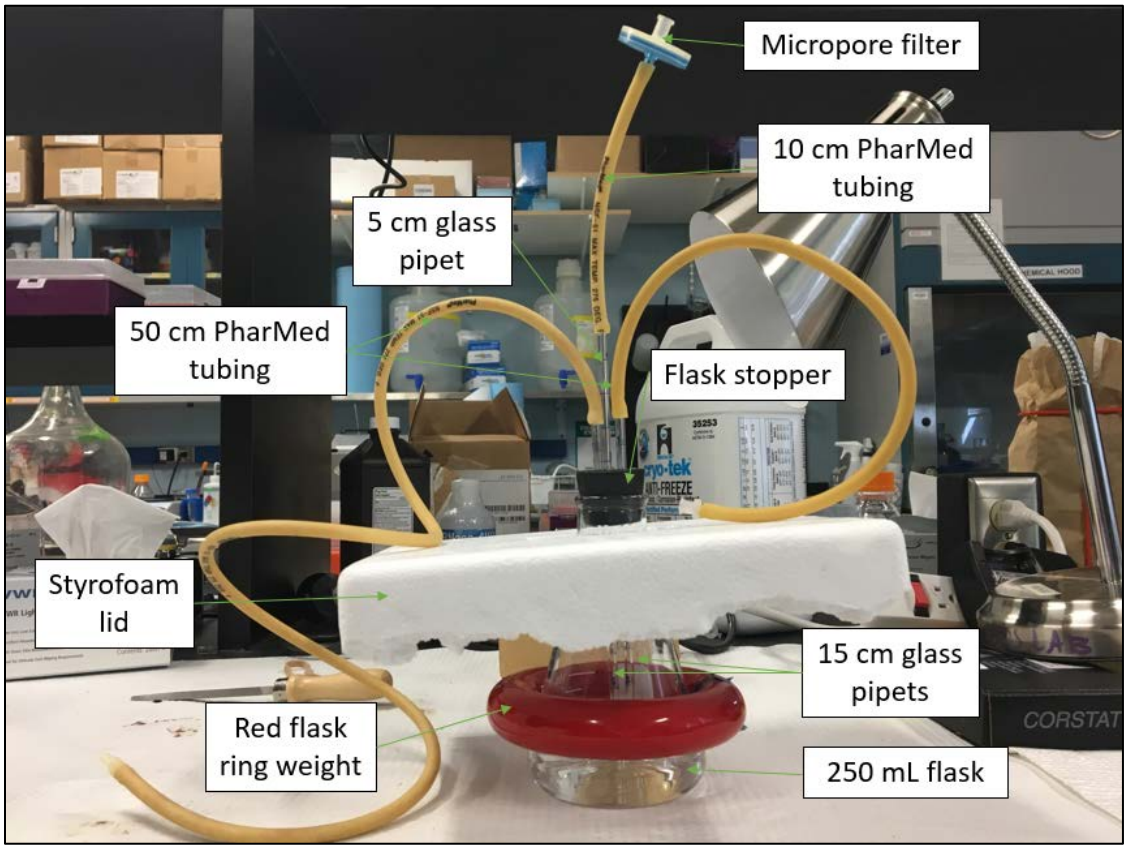

Figure 16: Completed Reservoir. Components from Table 3 are labeled appropriately.

Once the reservoir is complete, the flow loop is next to be assembled. Connect one 50 cm length of PharMed tubing to either 50 cm length connected to the reservoir. Clip this piece of tubing into the peristaltic pump. Then, connect the tubing to the perfusion tube assembly. Connect the other 50 cm PharMed tube attached to the reservoir to the opposite port of the perfusion tube assembly. The resultant loop should look identical to the loop in Figure 17. Set the peristaltic pump to a flow rate less than 0.1 mL/s. Place the perfusion tube assembly upside-down on top of a 250 mL beaker so that the perfusion tubes are facing down. Run the pump until media starts to flow out of the inlet tube. Continue to run the pump for 30 seconds while adjusting the PharMed tubing to ensure there are no bubbles in the lines. Once all of the bubbles have been removed, the chamber can be assembled.

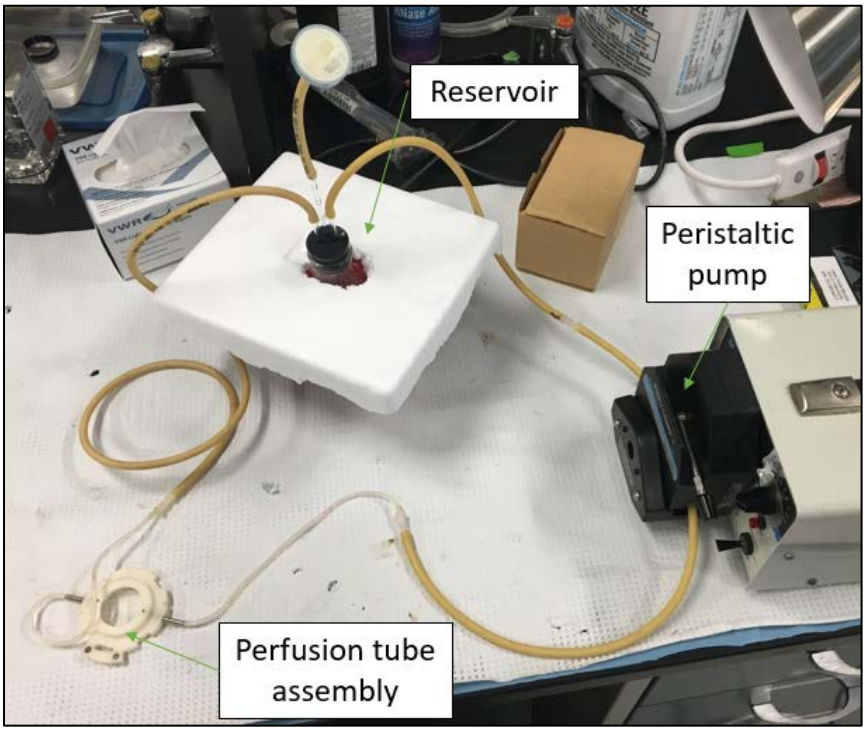

Figure 17: Completed flow loop. At this stage, tubes leading from the reservoir to the inlet perfusion tube should be completely free of air.

Using the forceps, place the upper gasket onto the perfusion tube assembly, ensuring the perfusion tubes poke through the holes in the gasket. Place the microaqueduct slide on top of the upper gasket, aligning the holes in the slide with the perfusion tubes. Place the thin lower gasket onto the slide so that the rectangular cut spans the gap between the T-shaped cuts in the microaqueduct slide. Place the thick lower gasket on top of the thin lower gasket. Using the forceps to hold the gaskets in place, turn on the pump to a flow rate below 0.1 mL/s and allow the empty space created by the gaskets to be filled with media. Remove the cell-cultured cover slip from the incubator. Verify using a phase microscope that the endothelial cells have formed a confluent layer. After spraying the culture dish containing the cover slip with 70% ethanol, bring the dish under the sterile laminar flow hood. Use the forceps to remove the cover slip from the culture dish and flip it cell-side down on top of the thick lower gasket. Loosen the self-locking base all of the way, and then place it on top of the chamber assembly. Carefully grab the chamber from underneath and flip it over so that the perfusion tube assembly is facing up, ensuring that the gasket

layers do not shift. Turn the ring on the self-locking base to seal the flow chamber. The sealed chamber should look like Figure 18.

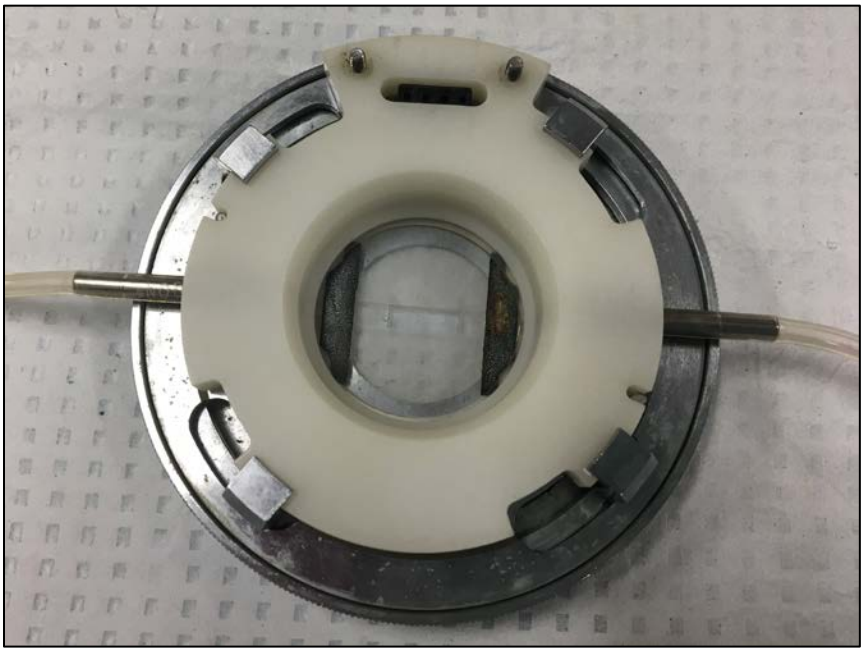

Figure 18: Sealed flow chamber. Note the step flow geometry created by the layered lower gaskets

Remove the completed flow loop from the laminar flow hood and take the loop to the microscope. Slide the FCS2 chamber into the base and tighten the screw to lock the chamber into place. Attach the electrical enclosure to monitor temperature. Place the reservoir into the water bath and tape the Styrofoam lid over the water bath. Set the peristaltic pump next to the microscope and above the water bath. Set the pump to 0.3 mL/s and turn it on. Verify using the microscope that the endothelial cells are still adhered to the cover slip and that the fluorescent beads are flowing through the chamber. Check the chamber for any leaks. The completely assembled flow loop on the microscope is displayed in Figure 19.

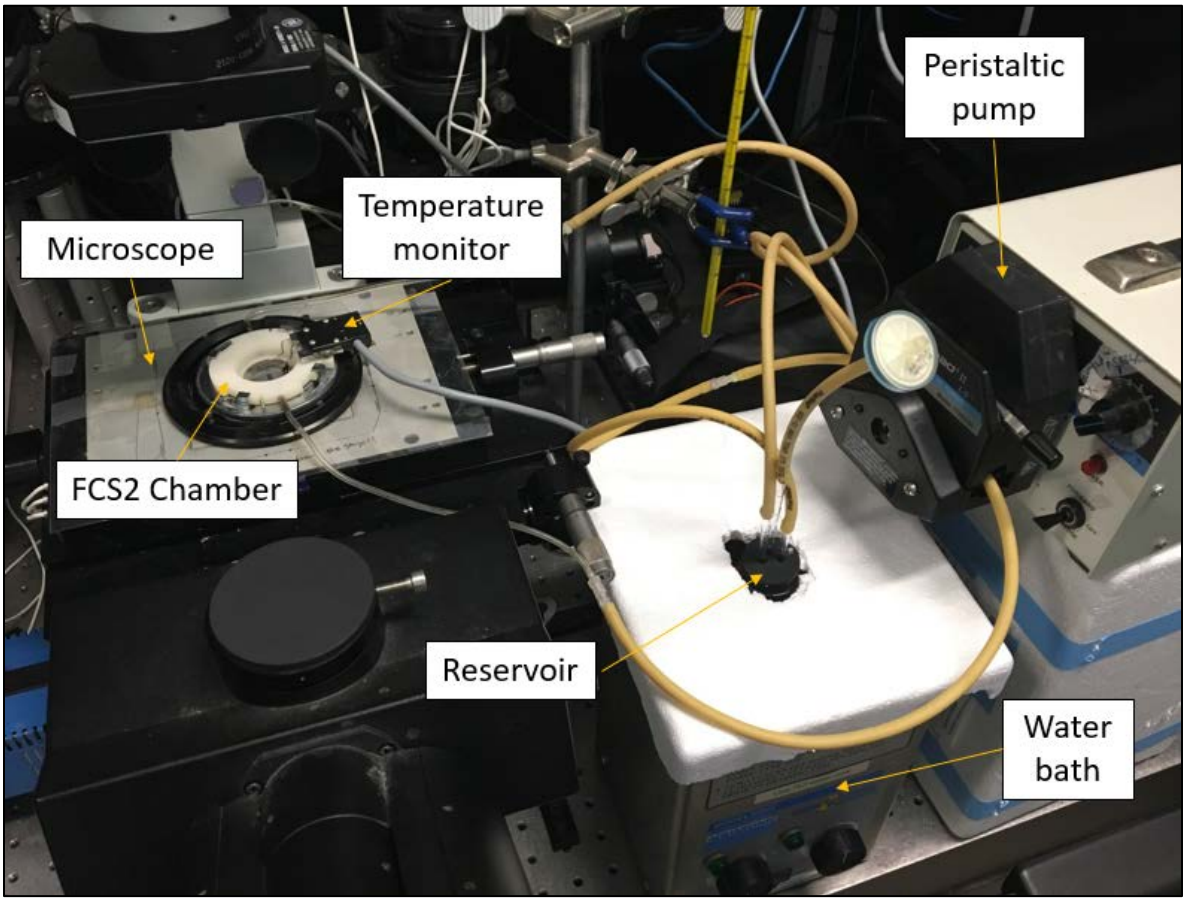

Figure 19: Completed experimental setup. Water bath and temperature monitor ensure the temperature of the chamber is held at the necessary 37 degrees Celsius.

Section 4.4 – Imaging and Analysis

Once flow loop assembly is competed, three testing zones are selected for imaging. The first zone is the low shear recirculation region, the second is the flow reattachment, and the third is the high shear aligned flow region. These regions are determined by visual inspection and their position according to the microscope stage micrometer is recorded. One image is taken at each region before once the flow loop is turned on. These regions are then imaged every 6 hours for 24 hours. The fluorescence intensity of each region at each time point, an indicator of the number of nanoparticles endocytosed by the endothelial cells, is measured using ImageJ image analysis software. The fluorescence intensity values for each

region at each time are compared. A t-test is performed to determine whether the fluorescence intensity values were significantly different.

Chapter 5

RESULTS

Preliminary data from the Comsol Modeling phase of this project indicates favorable results for the proposed flow chamber. The tested geometry fulfills all four design needs: flow recirculation, inclusion of a porous matrix, ability to culture cells within the chamber, and the ability to image the chamber with high resolution microscopy in real time. These fulfilled needs will be discussed in greater detail in the following sections.

Section 5.1 – Steady-State Flow Study

The steady-state laminar flow and porous media flow Comsol study yielded encouraging results. The streamline plot of the flow is shown in Figure 21. Note the regions of recirculation near the chamber expansion. Figure 20 displays the fluid shear stress of the computational model as a function of x-position along the bottom of the chamber. Note that the shear stress in the recirculation region (up to x = 2.6 mm) is very low. The stress spikes to a maximum of 20 dynes/cm^2 shortly after the flow reattachment and then levels out to around 8 dynes/cm^2. Cells in the recirculation region should display a spread morphology due to the low shear stress, while cells after the flow reattachment should display an aligned morphology. Figure 22 is a zoomed-in view of the streamline plot. This demonstrates that there is flow through the porous matrix. This flow through the porous matrix will help to create interstitial flow in the flow chamber and help to draw nanoparticles into the endothelial cells.

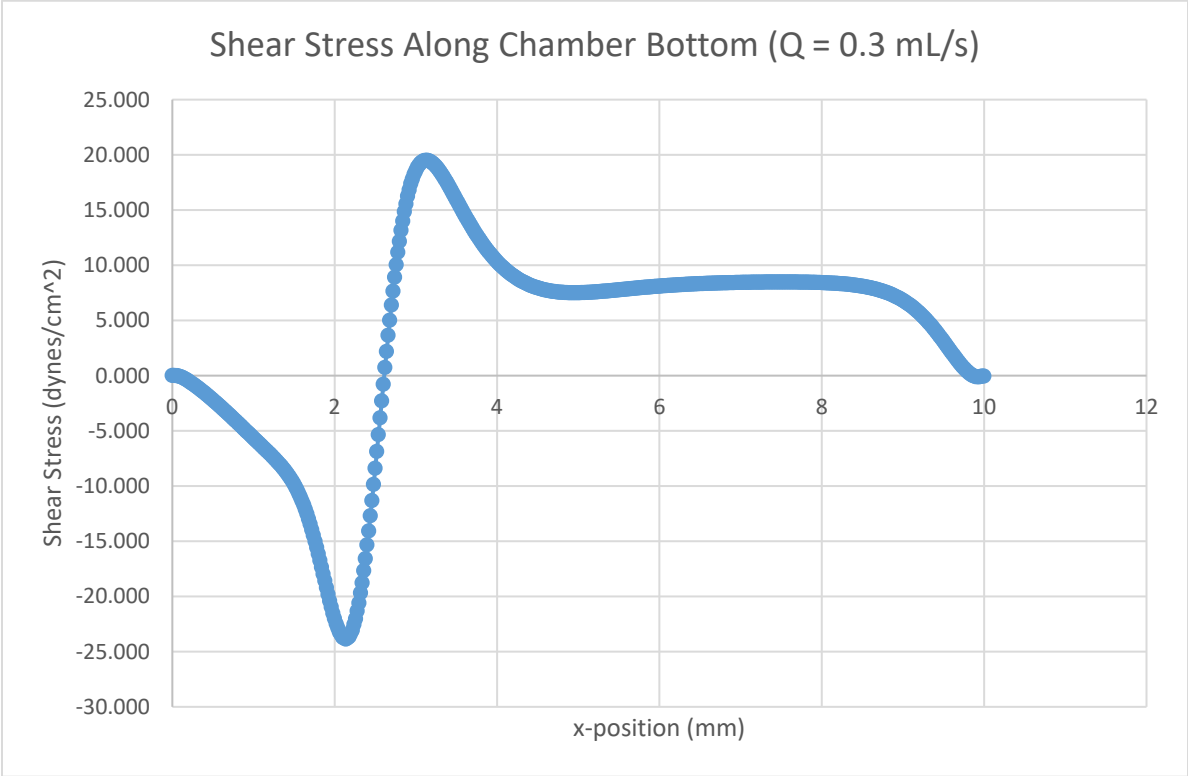

Figure 20: Fluid shear stress profile along bottom of flow chamber. Reattachment of flow occurs at x = 2.6 mm where the plot crosses 0 dynes/cm^2.

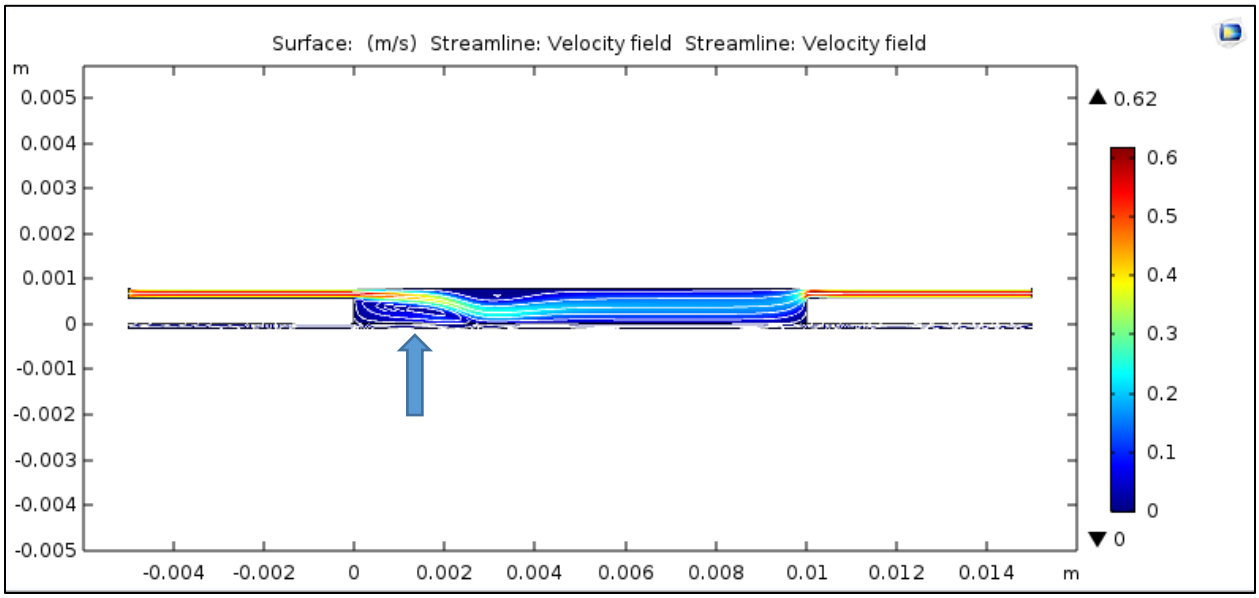

Figure 21: Streamline plot of flow with high flow velocity in red and low velocity in dark blue. Note the recirculation region near the inlet, indicated by the arrow.

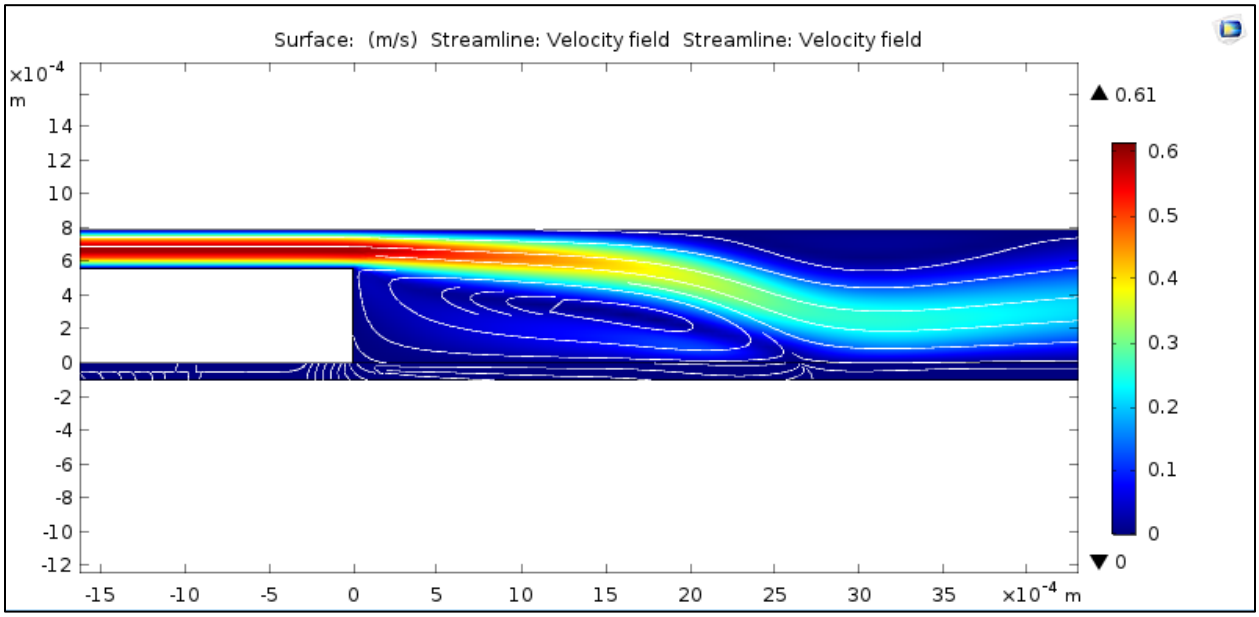

Figure 22: Zoomed-in streamline plot. Streamlines clearly flow into the porous media at the flow reattachment point and directly to the right of the step.

This portion of the study has two key learnings. First, the expansion of the chamber is sufficient to create a large recirculation zone. Next, the streamlines travel down through the gel-fluid interface and through the gel, creating an interstitial flow. The 100 μm thick gel is sufficiently small enough to afford the possibility of imaging the cells on top of the gel. The steady-state study shows that all of the four design goals can be met with one chamber design.

Section 5.2 – Transient Particle Tracing Study

The transient particle tracing simulation indicates that the recirculation region has an impact on where more particle uptake is highest. Figure 21 demonstrates time points at which particle trajectories are of interest. Following the 1.5 s simulation, three particles have stuck to the porous media in the recirculation while only one has stuck in the linear flow region. This trend was found to be consistent across ten simulations. Over the ten simulations, a minimum of three and a maximum of seven particles

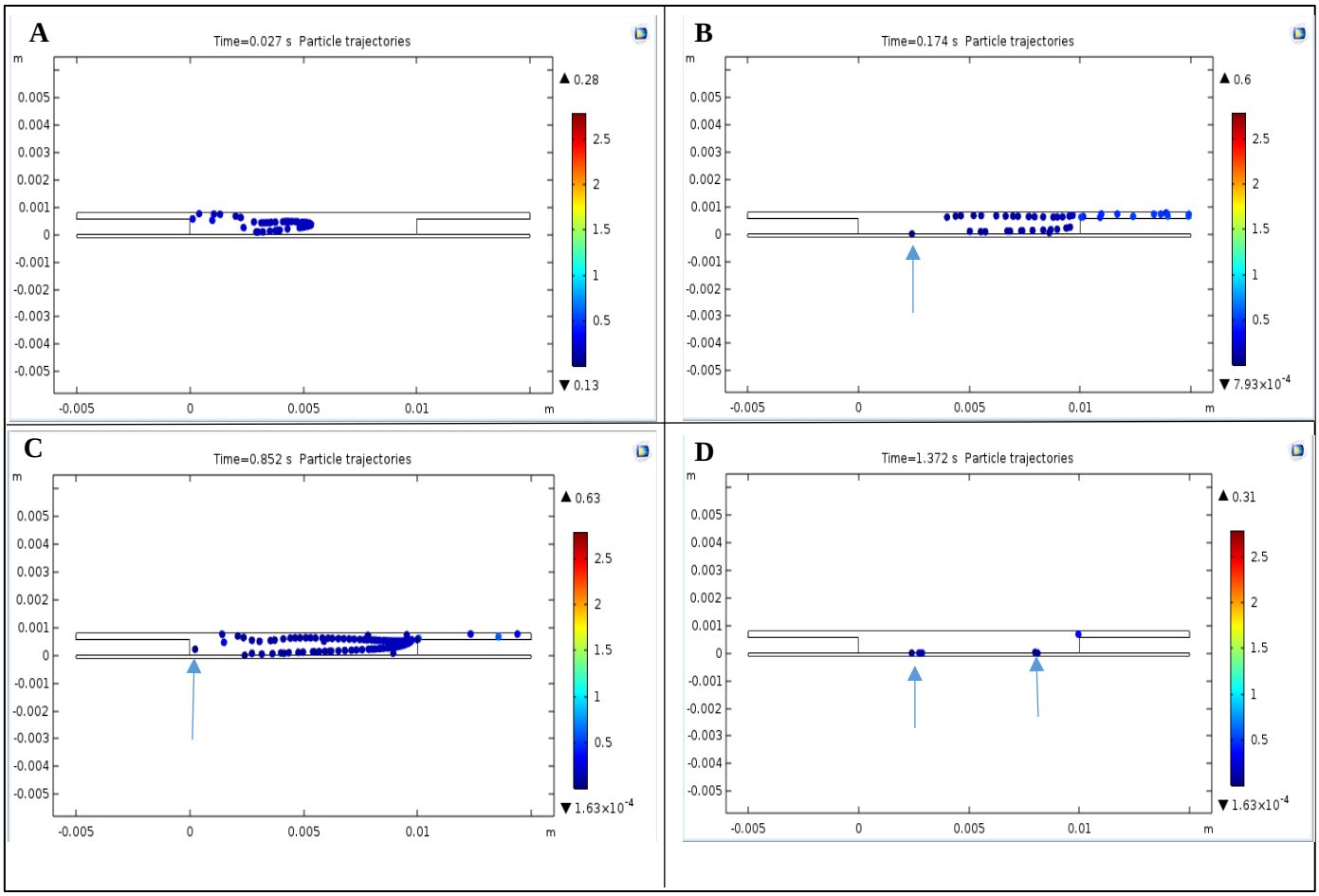

Figure 23: Particle trajectory at 4 time points. *A*: t = 0.027 s. Particles enter chamber with parabolic profile characteristic of laminar flow. *B*: t = 0.174 s. First particle sticks to gel-fluid boundary, labeled by arrow. *C*: t = 0.852. A particle (labeled by arrow) enters recirculation region while rest of particles pass through chamber. *D*: t = 1.372 s. Three particles stick in recirculation region compared to one in linear flow region following final particle release.

were observed to stick to the porous media in the recirculation zone. Conversely, no more than one particle was observed to stick in the aligned flow region over the ten simulations. On some simulations, particles also stuck in the small recirculation region in the rear of the chamber.

Section 5.3 – 3D Printing of Flow Chamber Gasket Investigation

Manufacturing the flow chamber gaskets using additive manufacturing technology proved to be a very difficult task. The compliant filament caused the extruder to jam up, resulting in multiple failed attempts at printing the gasket (Figure 24). Upon slowing down the print speed from 15 mm/s to 1 mm/s,

the gasket could be printed without jamming the extruder. However, the extremely slow printing speed resulted in abnormally large printing fibers and poor resolution overall. The resulting gasket, shown in Figure 25, is not suitable for use in this experiment. The crevices formed by the abnormally large fibers will allow fluid to flow and will prevent a tight seal in the FCS2 chamber. As a result, flow will not be constrained only to the cavity formed by the empty space in the gasket.

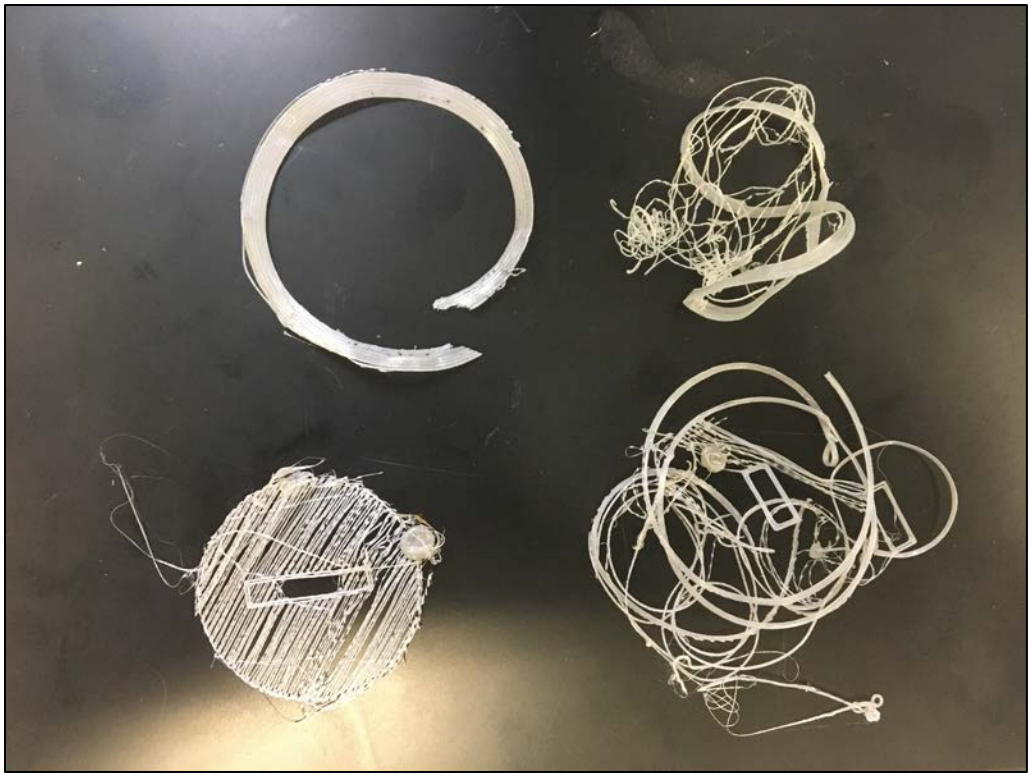

Figure 24: Failed 3D printing attempts due to a jammed extruder. Extruder took much longer to jam when flow through extruder was reduced by about half (lower left gasket), but filaments did not connect. Slowing the printing speed down from 15 mm/s gave better results.

This investigation indicates that extrusion-style printers are not suitable for this application. Because inkjet-style printers have shown success in the past, they should be considered further for this application. However, since the laser cutting method has proven adequate for manufacturing the flow chamber gaskets (figure 12), it is recommended that this be the primary technique used moving forward.

Figure 25: 3D printed gasket with 1 mm/s printing speed. Print was aborted after excessive filament size and low resolution were observed.

Section 5.4 –Preliminary Results from Flow Chamber Study

Preliminary results indicate the flow chamber behaves nearly identically to the computational model. Figure 26 displays three frames from a recording of the flow next to the inlet. During this recording, the pump was set to a flow rate of 0.03 mL/s. The flow reattachment can easily be identified by the bifurcation in particle trajectory. Particles on the right side of the reattachment in the recirculation zone travel from left to right at a low velocity and start to travel upwards away from the camera when they reach the rear wall. Particles on the left side of the reattachment point travel from right to left at a very high velocity. The reattachment point was measured in ImageJ to be 0.446 mm from the inlet. When the computational model was set to the same conditions, the reattachment point was measured at 0.44 mm (Figure 27).

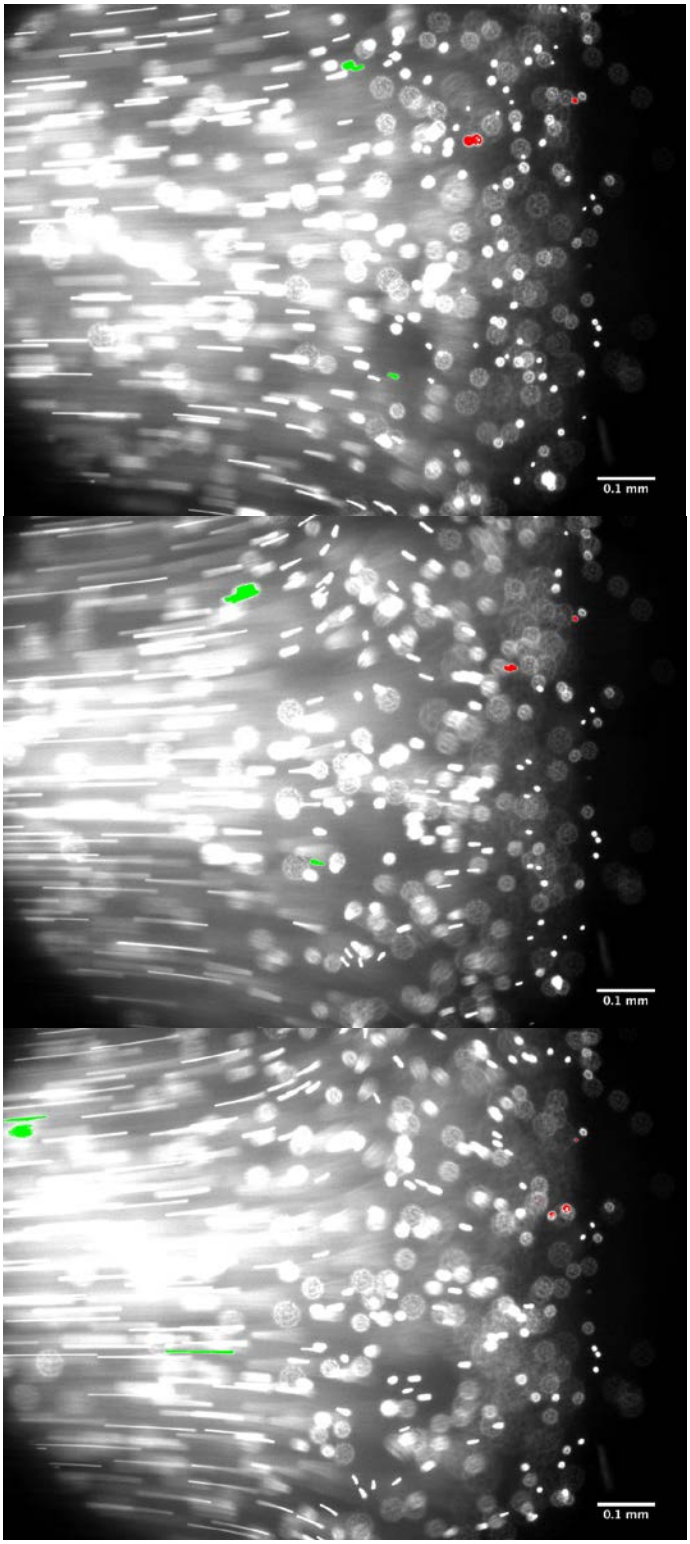

Figure 26: Three frames from flow recording. Particles in recirculation zone are labeled in red and particles in aligned flow are labeled green. Note that the particles in the recirculating flow travel left to right and upward away from the camera. Conversely, the particles in the aligned flow travel right to left and at a much higher velocity, indicated by the motion blur.

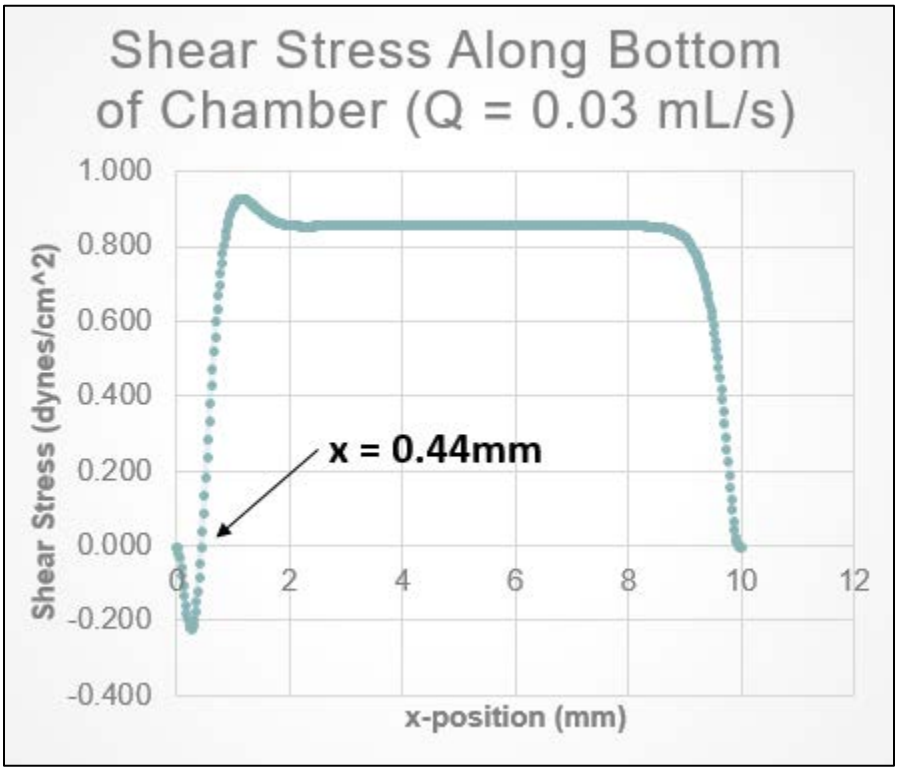

Figure 27: Shear stress profile for flow rate of 0.03 mL/s. Reattachment point occurs where curve crosses 0 at x = 0.44 mm.

The fact that the manufactured FCS2 flow chamber measures so closely with the computational model is very encouraging. Data up to this point suggests that the flow conditions in the chamber and the model are comparable. Due to a variety of complications including mistakes during the flow loop assembly process and the availability of endothelial cells, suitable data to compare the transport properties of the endothelial cells to the results from the model has not yet been collected. Three attempts were made at running the full 24 hour study. In each instance, air bubbles that went undetected during the assembly process sheared away cells from the cover slip.

Chapter 6

CONCLUSIONS AND FUTURE DIRECTIONS

Developing an effective method for drug delivery to atherosclerotic lesions continues to be one of the main challenges in mechanotransduction and cardiovascular engineering. This work provides encouraging preliminary data that the mechanical conditions that drive the pathology of atherosclerosis may be the key to unlock drug delivery methods.

Computational modeling was utilized to drive the design of a flow chamber to test the hypothesis that cells in flow recirculation regions uptake more nanoparticles than cells in aligned flow regions. Through modeling in Comsol, the main geometry of the chamber was tested and confirmed, and all of the design goals were met. Data from the particle tracing simulation suggests that cells will uptake more nanoparticles in flow recirculation regions. Further work can be competed in order to create a more robust computational model. Presently, transport of diluted species is not simulated and instead nanoparticle uptake is simulated through the “freeze” function of the wall boundary condition. This simulation is reasonable for preliminary data collection, but it is ultimately recommended that the transport of diluted species physics simulation be worked into the model in the future.

Data from the flow chamber suggests the chamber behaves very similarly to the computational model. However, data on nanoparticle uptake has not presently been collected. Three failed attempts at the experiment have helped to determine the appropriate assembly process presented in the Methods section of this thesis. There are several takeaways that can be gleaned from the attempted experiments. Endothelial cells were successfully seeded on the coverslip and the chamber was assembled on multiple occasions without contamination. The desired flow conditions (recirculating and aligned flow) were observed and easily identified within the chamber. This is strong evidence that the hypothesis presented in this thesis certainly can be tested with the proposed chamber as long as the protocol is followed correctly.

Though a lot of progress was made towards testing the hypothesis that nanoparticle uptake is modulated by cellular mechanics as a result of flow conditions, there is still work to be done. The key moving forward is a careful and deliberate approach to the flow loop assembly to ensure that the flow loop is completely free of air that will damage the endothelial cells. Additionally, the polyacrylamide gel still needs to be integrated into the chamber for traction force microscopy.

Some future directions for this experiment include, but are not limited to: performing nanoparticle uptake experiments with a blood analog; modifying the injected nanoparticles to change their Sherwood and Damkohler Numbers and evaluating the effect this has; and functionalizing nanoparticles with adhesion molecules to see if this increases their absorption efficiency. This project has an exciting future with critical ramifications for cardiovascular disease treatment.

Appendix A

Silicon Gasket Dimensions

Engineering drawings of each variation of the flow chamber gaskets are displayed below. Figure A-1 shows the top view of the thicker bottom gasket and the dimensions of the cut. Figure A-2 shows the top view of the thinner top gasket and the dimensions of the cut. A top view of the 3D printed gasket is shown in Figure A-3. The same gasket is shown in a side view in Figure A-4.

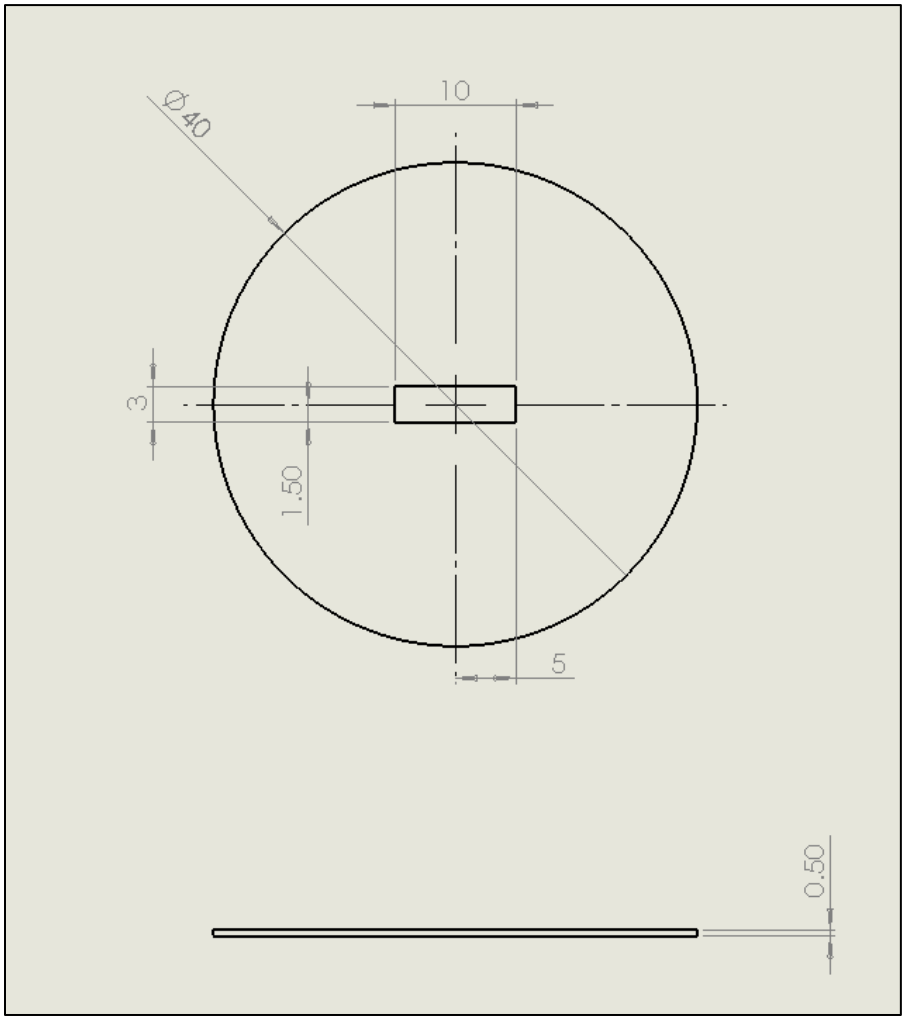

Figure A-1: Engineering drawing of laser cut bottom gasket with dimensions of cut displayed

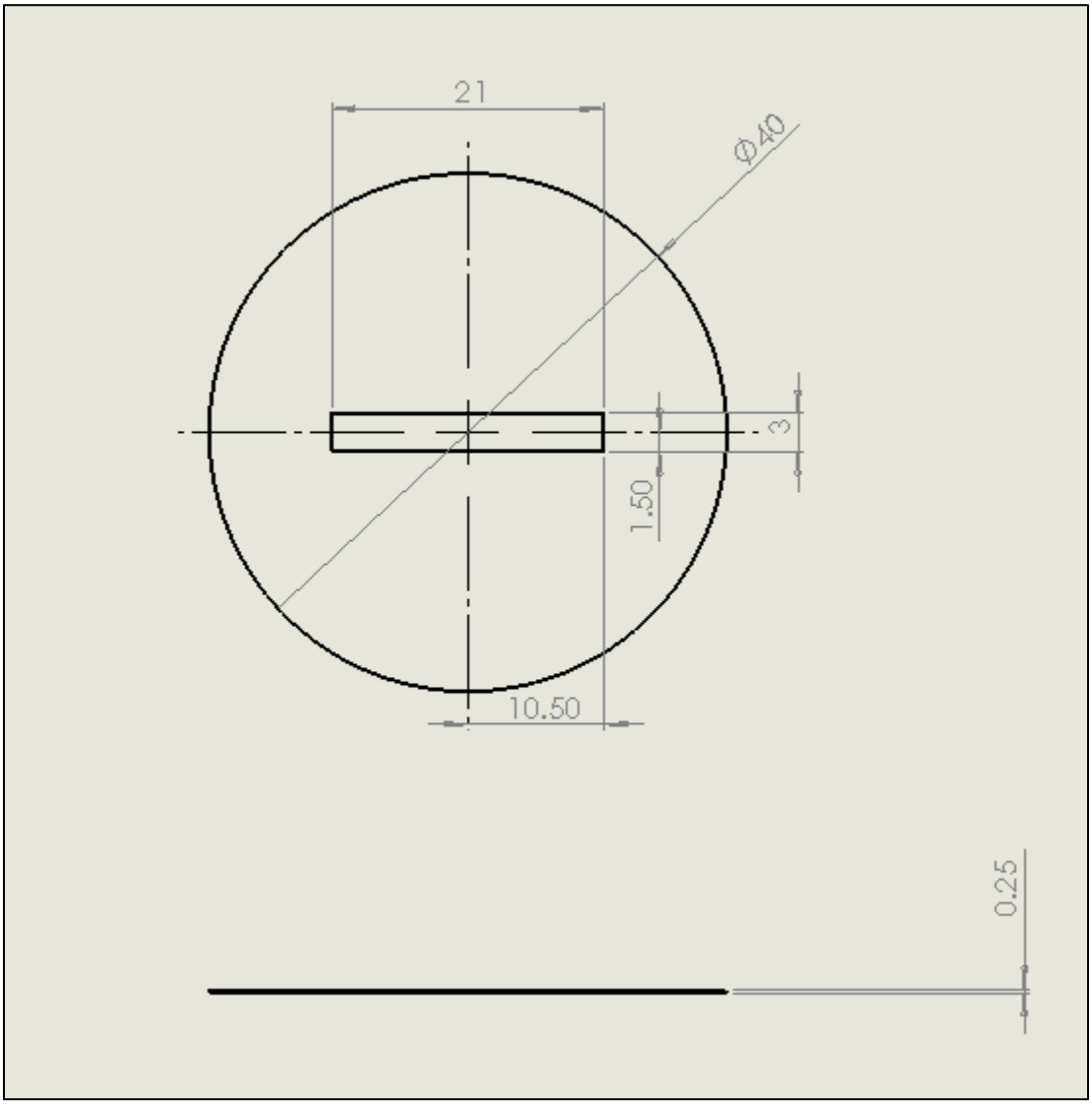

Figure A-2: Engineering drawing of laser cut top gasket with dimensions of cut displayed

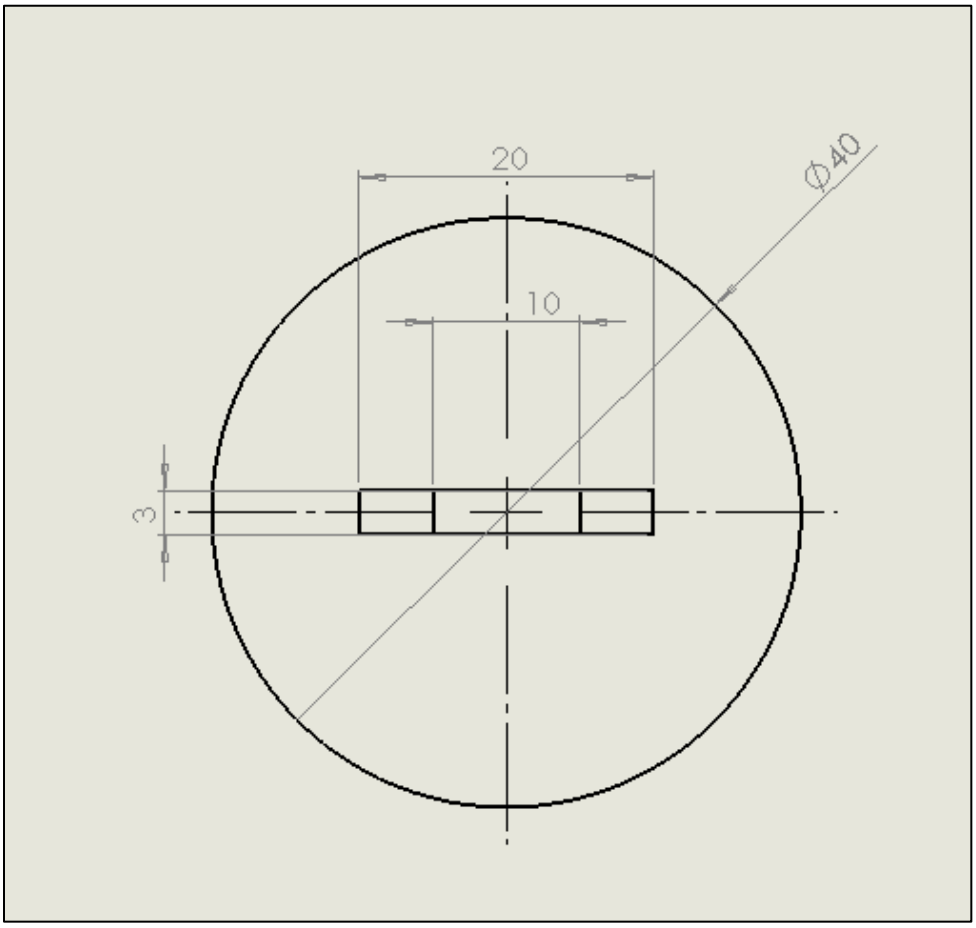

Figure A-3: Engineering drawing of top view of CAD model for 3D printed gasket with relevant dimensions displayed.

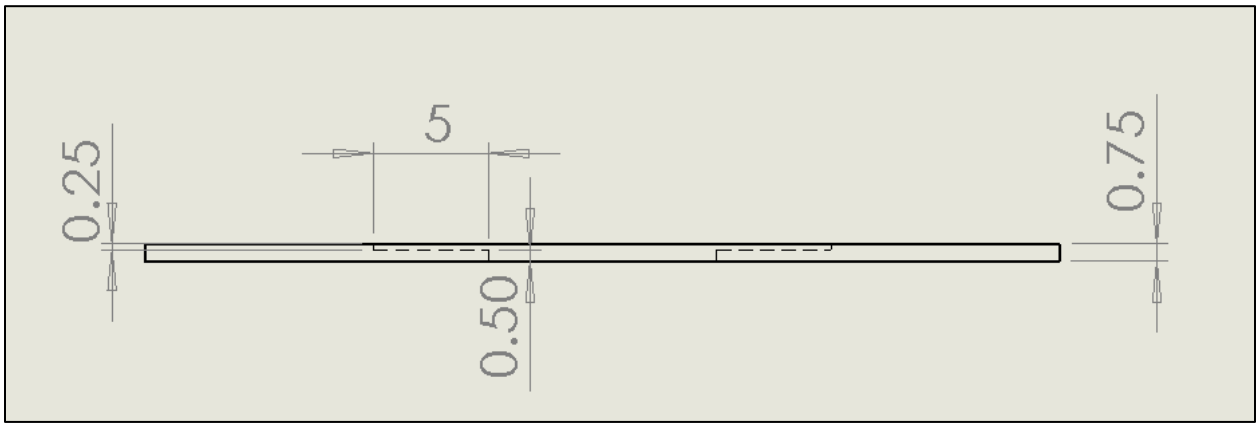

Figure A-4: Engineering drawing of side view of CAD model 3D printed gasket with relevant dimensions displayed.

Appendix B

Traction Force Microscopy Gel Protocol

Making Polyacrylamide gel substrate

Materials:

- 3-Aminopropyl-trimethoxysilane (Sigma, St. Louis , MO)
- Glutaraldehyde stock solution (25%)
- Ammonium Persulfate
- Acrylamide (40%), Bis-acrylamide (2%)

Procedures**:**

Step 1: Treat coverslip (ensures PA gel can adhere onto coverslip)

Method 1:

1. Dilute Poly-D-Lysine into 0.1mg/ml
2. Pipet 100ul Poly-D-Lysine (0.1mg/ml) onto coverslip and cover the drop with parafilm to make the liquid spread on the coverslip
3. Wait for 1 hour and then remove the parafilm and Poly-D-Lysine

Method 2:

1. First clean the hotplate: Use Isopropanol, DI water (in sequence) and wipe with sterilized paper towels.
2. Set the temperature of the hotplate to 160 ^{o}C (110 ^{o}C for Petri dishes) and sterilize for 10 minutes.

3. Use a 10 cm Petri dish to cut out circular shapes from the sterilized paper towels and insert them into several large Petri dishes.
4. Place glass cover slides on the hotplate and heat them for 15 minutes.
5. During the wait, prepare a 1% glutaraldehyde solution (0.4mL glutaraldehyde + 10mL DI water).
6. After waiting 15 minutes, remove the cover slides from the hotplate and place them into the Petri dishes with paper inserts prepared in step 3. Cover each slide with 2% 3-Aminopropyl-trimethoxysliane (original concentration >=99.5%). Put just enough solution (400ul, use syringe and glass pipette) to cover the top of the slide. Wait for 7 minutes for chemical activation.
7. Wash the cover slide with DI water (3 times, 5 minutes for each time) and place it onto the hot plate with the activated side facing up. Wait for 20 minutes.
8. Remove the cover slides from the hotplate and place them back into large Petri dishes with new paper inserts. Cover the top of each slide completely with the 1% glutaraldehyde solution (800ul) prepared in step 4a. Wait for 30 minutes.
9. After the 30-minute wait wash the slides with DI water three times and dry

Step 2: Treat glass slide

1. Wipe the glass slide hardly with X-rain (This step is very important which makes glass slide super hydrophobic)

Step 3: Make gel

1. Prepare pre-polymerization solution for gel with different stiffness. The formation of pre-polymerization solution is shown in the attached table.

2. Place 500ul mixture pre-polymerization solution mixture into the vacuum jar and turn on the vacuum to prevent early polymerization.
3. Remove the gel mixture from the vacuum chamber and quickly add 0.8uL TEMED and 2.5uL of ammonium persulfate (10mg crystal + 100uL DI water = 10% solution. Solution must be used within 30 minutes). Immediately pipet the mixture (35uL for a 24X24mm coverslip) onto the treated glass slide, and cover with treated coverslips. Wait 30 minutes for gel formation.
4. After waiting for gel formation remove the top coverslip and place each gel into a petri-dish and submerge in DI water. Wash two times (5 minutes for each time) using DI water.

Coupling extracellular matrix (ECM) proteins to the PAA gel

Materials:

- Sulfo-SANPAH. 50mg Sulfo-SANPAH powder is made to be 50mg /ml by adding 1000ul DMSO. Store it in -20^{o}C and handle it in the dark.
- HEPES, 50mM, PH8.5, 500ml. Use at room temperature.
- DMSO
- Fibronectin at 0.5 mg/ml in PBS. Dilute the stocking fibronectin solution to 50 ug/ml with PBS.
- PBS (PH 7.4)

Procedures:

1. Move out the gel, remove ddH_20 from gel surface as much as possible (avoiding drying the gel) and transfer it to another dry petri-dish

2. Dilute Sulfo-SANPAH-DMSO aliquots in HEPES (50mM, pH 8.5) to reach 0.5mg/ml immediately before use, vortex and pipet 250ul solution onto gel surface (make sure Sulfo-SANPAH cover all the area of gel). Note that the reactivity half-life of Sulfo-SANPAH is short (~5 min) at room temperature in water; therefore, these steps should be done at a rapid pace.
3. Expose gel surface to UV light under a UV cross-linker lamp (6W, 365 nm wavelength at a distance of 2-3 inches for 20 min). Sulfo-SANPAH will change in color from orange to brown.
4. Wash gel two times using 50mM HEPES and one time using PBS.
5. In biological hood, move out the gel, remove PBS from gel surface as much as possible (avoiding drying the gel) and transfer it to a new petri-dish.
6. Pipet 250ul fibronectin (50ug/ml) on to the gel surface.
7. Move the petri-dish including gel to a sterilized large glass petri-dish, wrap it with aluminum foil paper and incubate it in fridge overnight.
8. The next day, move large glass petri-dish to biological hood, move out petri-dish including gel and then wash gel with PBS three times.
9. Sterile the gel in biological hood using UV light for 30 minutes.

BIBLIOGRAPHY

1. Lusis, A. J. (2000). Atherosclerosis. *Nature*, *407*(September), 233–241. http://doi.org/10.1038/35025203
2. Falk, E. (2006). Pathogenesis of Atherosclerosis. *Journal of the American College of Cardiology*. http://doi.org/10.1016/j.jacc.2005.09.068
3. Green, D. (2006). Coagulation cascade. In *Hemodialysis International* (Vol. 10). http://doi.org/10.1111/j.1542-4758.2006.00119.x
4. Aschoff L. Thrombose und Sandbankbildung. Be- itr Path Anat. 1912;52:205-212.
5. Malek, A. M. (1999). Hemodynamic Shear Stress and Its Role in Atherosclerosis. *JAMA*, *282*(21), 2035. http://doi.org/10.1001/jama.282.21.2035
6. Fry DL. Certain histological and chemical responses of the vascular interface to acutely induced mechanical stress in the aorta of the dog. Circ Res. 1969;24:93-108.
7. Insull, W. (2009). The Pathology of Atherosclerosis: Plaque Development and Plaque Responses to Medical Treatment. *American Journal of Medicine*, *122*(1 SUPPL.). http://doi.org/10.1016/j.amjmed.2008.10.013
8. Ku, D. N., Giddens, D. P., Zarins, C. K., & Glagov, S. (1985). Pulsatile flow and atherosclerosis in the human carotid bifurcation. Positive correlation between plaque location and low oscillating shear stress. *Arteriosclerosis, Thrombosis, and Vascular Biology*, *5*(3), 293–302. http://doi.org/10.1161/01.ATV.5.3.293
9. Koskinas, K. C., Feldman, C. L., Chatzizisis, Y. S., Coskun, A. U., Jonas, M., Maynard, C., … Stone, P. H. (2010). Natural history of experimental coronary

atherosclerosis and vascular remodeling in relation to endothelial shear stress: A serial, in vivo intravascular ultrasound study. *Circulation*, *121*(19), 2092–2101. http://doi.org/10.1161/CIRCULATIONAHA.109.901678

10. Dangaria, J. H., & Butler, P. J. (2007). Macrorheology and adaptive microrheology of endothelial cells subjected to fluid shear stress. *American Journal of Physiology. Cell Physiology*, *293*(5), C1568-75. http://doi.org/10.1152/ajpcell.00193.2007

11. Goldfinger, L. E., Tzima, E., Stockton, R., Kiosses, W. B., Kinbara, K., Tkachenko, E., … Ginsberg, M. H. (2008). Localized α4 integrin phosphorylation directs shear stress-induced endothelial cell alignment. *Circulation Research*, *103*(2), 177–185. http://doi.org/10.1161/CIRCRESAHA.108.176354

12. McCue, S., Noria, S., & Langille, B. L. (2004). Shear-induced reorganization of endothelial cell cytoskeleton and adhesion complexes. *Trends in Cardiovascular Medicine*. http://doi.org/10.1016/j.tcm.2004.02.003

13. Gavara, N., & Chadwick, R. S. (2016). Relationship between cell stiffness and stress fiber amount, assessed by simultaneous atomic force microscopy and live-cell fluorescence imaging. *Biomechanics and Modeling in Mechanobiology*, *15*(3), 511–523. http://doi.org/10.1007/s10237-015-0706-9

14. Singh, R., & Lillard, J. W. (2009). Nanoparticle-based targeted drug delivery. *Experimental and Molecular Pathology*. http://doi.org/10.1016/j.yexmp.2008.12.004

15. Moghimi, S.M., Hunter, A.C., Murray, J.C., 2001. Long-circulating and target-specific nanoparticles: theory to practice. Pharmacol. Rev. 53, 283–318.

16. Zhang, S., Gao, H., & Bao, G. (2015). Physical Principles of Nanoparticle Cellular Endocytosis. *ACS Nano*. http://doi.org/10.1021/acsnano.5b03184

17. Huang, C. J.; Butler, P. J.; Tong, S.; Muddana, H. S.; Bao, G.; Zhang, S. L. Substrate Stiffness Regulates Cellular Uptake of Nanoparticles. Nano Lett. 2013, 13, 1611–1615. 118.

18. Tarbell, J. M. (2003). Mass Transport in Arteries and the Localization of Atherosclerosis. *Annual Review of Biomedical Engineering*, *5*(1), 79–118. http://doi.org/10.1146/annurev.bioeng.5.040202.121529

19. Iyer, A. K., Khaled, G., Fang, J., & Maeda, H. (2006). Exploiting the enhanced permeability and retention effect for tumor targeting. *Drug Discovery Today*. http://doi.org/10.1016/j.drudis.2006.07.005

20. Poole, R. J., Pinho, F. T., Alves, M. A., & Oliveira, P. J. (2009). The effect of expansion ratio for creeping expansion flows of UCM fluids. *Journal of Non-Newtonian Fluid Mechanics*. http://doi.org/10.1016/j.jnnfm.2009.06.004

21. Yu, H.-S., Won, J.-E., Jin, G.-Z., & Kim, H.-W. (2012). Construction of mesenchymal stem cell-containing collagen gel with a macrochanneled polycaprolactone scaffold and the flow perfusion culturing for bone tissue engineering. *BioResearch Open Access*. http://doi.org/10.1089/biores.2012.0234

22. Jabaji, Z., Sears, C. M., Brinkley, G. J., Lei, N. Y., Joshi, V. S., Wang, J., … Dunn, J. C. Y. (2013). Use of collagen gel as an alternative extracellular matrix for the in vitro and in vivo growth of murine small intestinal epithelium. *Tissue Engineering. Part C, Methods*, *19*(12), 961–9. http://doi.org/10.1089/ten.TEC.2012.0710

23. Sharif, D., Sharif-Rasslan, A., Shahla, C., Khalil, A., & Rosenschein, U. (2015). Differences in coronary artery blood velocities in the setting of normal coronary angiography and normal stress echocardiography. *Heart International*, *10*(1), e6–e11. http://doi.org/10.5301/heartint.5000221

24. Powell, J. T. (1998). Vascular damage from smoking: disease mechanisms at the arterial wall. *Vascular Medicine (London, England)*, *3*, 21–28. http://doi.org/10.1191/135886398670269973

25. Chang, E., & Abe, J. I. (2016). Kinase-SUMO networks in diabetes-mediated cardiovascular disease. *Metabolism: Clinical and Experimental*. http://doi.org/10.1016/j.metabol.2016.01.007

26. Lobatto, M. E., Fuster, V., Fayad, Z. A., & Mulder, W. J. M. (2011). Perspectives and opportunities for nanomedicine in the management of atherosclerosis. *Nature Reviews Drug Discovery*. http://doi.org/10.1038/nrd3578

27. Nahrendorf, M., Jaffer, F. A., Kelly, K. A., Sosnovik, D. E., Aikawa, E., Libby, P., & Weissleder, R. (2006). Noninvasive vascular cell adhesion molecule-1 imaging identifies inflammatory activation of cells in atherosclerosis. *Circulation*, *114*(14), 1504–1511. http://doi.org/10.1161/CIRCULATIONAHA.106.646380

28. Müller, K., Fedosov, D. A., & Gompper, G. (2014). Margination of micro- and nano-particles in blood flow and its effect on drug delivery. *Scientific Reports*, *4*. http://doi.org/10.1038/srep04871

29. Raub, C. B., Putnam, A. J., Tromberg, B. J., & George, S. C. (2010). Predicting bulk mechanical properties of cellularized collagen gels using multiphoton

microscopy. *Acta Biomaterialia*, *6*(12), 4657–4665. http://doi.org/10.1016/j.actbio.2010.07.004

30. "FCS2 System." *Bioptechs*. Bioptechs, www.bioptechs.com/product/fcs2-system/.

31. Tarbell, J. M. (2003). Mass Transport in Arteries and the Localization of Atherosclerosis. *Annual Review of Biomedical Engineering*, *5*(1), 79–118. http://doi.org/10.1146/annurev.bioeng.5.040202.121529

32. Perktold, K., Rappitsch, G., Hofer, M., and Karner, G., Numerical simulation of ass transfer in a realistic carotid artery bifurcation model, *Proceedings of the Bioengineering Conference (ASME), BED*, 35, 85, 1997.

33. Truskey, G. A., Roberts, W. L., Herrmann, R. A., & Malinauskas, R. A. (1992). Measurement of endothelial permeability to125I-low density lipoproteins in rabbit arteries by use of en face preparations. *Circulation Research*, *71*(4), 883–897. http://doi.org/10.1161/01.RES.71.4.883

34. Tarbell JM, Qiu Y. 2000. Arterial wall mass transport: the possible role of blood phase resistance in the localization of arte- rial disease. In The Biomedical Engineer- ing Handbook, ed. JD Bronzino, pp. 100– 15. New York: CRC. 2nd ed.

35. Tan, J., Thomas, A., & Liu, Y. (2012). Influence of red blood cells on nanoparticle targeted delivery in microcirculation. *Soft Matter*, *8*(6), 1934. http://doi.org/10.1039/c2sm06391c

36. Tan, J., Keller, W., Sohrabi, S., Yang, J., & Liu, Y. (2016). Characterization of Nanoparticle Dispersion in Red Blood Cell Suspension by the Lattice Boltzmann-Immersed Boundary Method. *Nanomaterials*, *6*(2), 30. http://doi.org/10.3390/nano6020030

37. Wang, J. H.-C., & Li, B. (2009). Application of cell traction force microscopy for cell biology research. *Methods in Molecular Biology (Clifton, N.J.)*, *586*, 301–13. http://doi.org/10.1007/978-1-60761-376-3_17

38. Zhao, T., Zhang, Y., Wei, Q., Shi, X., Zhao, P., Chen, L.-Q., & Zhang, S. (2018). Active cell-matrix coupling regulates cellular force landscapes of cohesive epithelial monolayers. *Npj Computational Materials*, *4*(1), 10. http://doi.org/10.1038/s41524-018-0069-8

39. White, M. L. (1960). The permeability of an acrylamide polymer gel. *Journal of Physical Chemistry*, *64*(10), 1563–1565. http://doi.org/10.1021/j100839a055

ACADEMIC VITA

Sam Boland
sfbol96@gmail.com

Education
Majors: B.S. – Biomedical Engineering, B.S. – Mechanical Engineering
Honors: Biomedical Engineering

Thesis Title: Investigating the Impact of Flow Recirculation on Cellular Uptake of Nanoparticles
Thesis Supervisor: Peter J Butler, PhD.

Work Experience:
06/2015 – present
Penn State Department of Biomedical Engineering
Cellular Mechanobiology Laboratory
Peter J. Butler, PhD.
Undergraduate Researcher
Utilize 3D printing and laser cutting techniques to manufacture novel flow chamber device to model drug delivery in bifurcated vasculature. Apply computational modeling principles to simulate nanoparticle uptake in the body and guide design of flow chamber. Designed, tested, and validated protocol for endothelial cell migration study used to investigate cellular adhesion.

06/2017 – 08/2017
W. L. Gore & Associates
Cory Donavon
Process & Quality Engineering Intern
Designed and executed experiments to determine appropriate parameters for new stent-graft manufacturing process in order to cut manufacturing time by 1.5 minutes per device. Used statistical Design Of Experiments (DOE) techniques to optimize existing manufacturing process in order to reduce material costs by $10,000/year. Investigated and resolved problems with Radio Frequency bonding equipment and improved vascular device yield by 20%. Drove Quality System documents to completion. Provided direct technical support to manufacturing operators. Shadowed and aided new product development associates in process development testing.

06/2016 – 08/2016
Summer Translational Cardiovascular Sciences Institute
Peter J. Butler, PhD.
Undergraduate Researcher
Integrated and improved previously untested method for measuring mechanics of cellular membranes to validate novel diagnostic equipment.

Grants Received: STCSI Summer Research Grant (Summer 2016), Schreyer Travel Grant (Spring 2016), Schreyer Summer Research Grant (Summer 2015).

Awards: Schreyer Honors College Academic Scholarship (Semesters 1-8), Dean's List (Semesters 1-3, 5-8)

Professional Memberships: Biomedical Engineering Society (2016 – present)

Presentations: Biomedical Engineering Society Annual Meeting Poster Presentation (October 2016), STCSI End of Summer Presentation (August 2016)

Community Service Involvement:
President, Apollo Benefiting THON (08/2014 – present)
Lead 100-person organization in philanthropic efforts for the Penn State Dance Marathon. Raised over $80,000 for pediatric cancer treatment and research. Develop new methods to raise money apart from established practices including Food Truck Festivals and Benefit Concerts. Facilitate weekly general body and Executive Board meetings.

International Engagement Committee Member, Global Ambassadors (08/2016 – present)
Helped organize inaugural International Buddy Campaign to partner incoming exchange students with American students to help aid assimilation process. Presented monthly to students interested in Studying Abroad about how to make experiences abroad more affordable.

SHO TIME Mentor, Schreyer Honors College (08/2015 – 08/2017)
Orientation leader for the Schreyer Honors College Class of 2019 & 2021. Facilitated ice-breaker activities over a course of 3 days. Spoke on panels regarding early research involvement and international experiences to an audience of first-year students.

Committee Volunteer, Penn State Dance Marathon (08/2015 – 02/2017)
Served as committee volunteer on Donor & Alumni Relations – Alumni Engagement and Special Events Committees. Coordinated parking efforts at THON-related events. Created decorations for Four-Diamonds Family-oriented events. Collected bottles and cans for THON Recycling and Environmental Effort (TREE) to raise funds for pediatric cancer. Distributed and collected envelopes for soliciting donations. Wrote thank you notes to alumni donors.

Secretary, Open The Box Campaign (08/2015 – 01/2015)
Co-lead campaign to bring sexual assault detection kits to Penn State's campus. Composed weekly emails to communicate with general body and executive board members. Communicated with media and student government organizations to spread awareness about the club's missions. Managed organization's Google Drive through the creation of documents and forms.

<u>International Education</u>:
01/2016 – 05/2016
University of Limerick, Limerick, Ireland.
Direct Enrollment – 15 credits